A RORγt+ cell instructs gut microbiota-specific Treg cell differentiation

Ranit Kedmi[1], Tariq A. Najar[1], Kailin R. Mesa[1], Allyssa Grayson[1,2], Lina Kroehling[1], Yuhan Hao[3,4], Stephanie Hao[5], Maria Pokrovskii[1,16], Mo Xu[1,17], Jhimmy Talbot[1,18], Jiaxi Wang[6], Joe Germino[6], Caleb A. Lareau[7,8,9], Ansuman T. Satpathy[7,8,9], Mark S. Anderson[6], Terri M. Laufer[10,11], Iannis Aifantis[12], Juliet M. Bartleson[13,19], Paul M. Allen[13], Helena Paidassi[14], James M. Gardner[6,15], Marlon Stoeckius[5,20], Dan R. Littman[1,2,†]

[1]Molecular Pathogenesis Program, The Kimmel Center for Biology and Medicine of the Skirball Institute, New York University School of Medicine, New York, NY, USA.

[2]Howard Hughes Medical Institute, New York, NY, USA.

[3]Center for Genomics and Systems Biology, New York University, New York, NY, USA.

[4]New York Genome Center, New York, NY, USA.

[5]Technology Innovation Lab, New York Genome Center, New York, NY, USA.

[6]Diabetes Center, University of California, San Francisco, San Francisco, CA, USA.

[7]Department of Pathology, Stanford University, Stanford, CA, USA.

[8]Parker Institute for Cancer Immunotherapy, Stanford University, Stanford, CA, USA.

[9]Gladstone-UCSF Institute of Genomic Immunology, San Francisco, CA, USA.

[10]Department of Medicine, Perelman School of Medicine, University of Pennsylvania, Philadelphia, PA, USA.

[11]Department of Medicine, C. Michael Crescenz Veterans Administration Medical Center, Philadelphia, PA, USA.

[12]Department of Pathology, New York University School of Medicine, New York, NY, USA.

[13]Department of Pathology and Immunology, Washington University School of Medicine, St. Louis, MO, USA.

[14]CIRI, Centre International de Recherche en Infectiologie, Université de Lyon, INSERM U1111, Université Claude Bernard Lyon 1, CNRS UMR5308, ENS de Lyon, Lyon, France.

[15]Department of Surgery, University of California, San Francisco, San Francisco, CA, USA.

[16]Current addresses: Calico Life Sciences, LLC, South San Francisco, CA, USA.

[17]National Institute for Biological Sciences, Beijing, China.

[18]Fred Hutchinson Cancer Center, Seattle, WA USA.

[19]Federation Bio, South San Francisco, CA, USA.

[20]10X Genomics, Stockholm, Sweden.

Abstract

The mutualistic relationship of gut-resident microbiota and the host immune system promotes homeostasis that ensures maintenance of the microbial community and of a largely non-aggressive immune cell compartment[1,2]. Consequences of disturbing this balance include proximal inflammatory conditions, like Crohn's disease, and systemic illnesses. This equilibrium is achieved, in part, through induction of both effector and suppressor arms of the adaptive immune system. *Helicobacter* species induce regulatory (iTreg) and follicular helper (Tfh) T cells under homeostatic conditions, but instead induce inflammatory Th17 cells when iTreg are compromised[3,4]. How *Helicobacter* and other gut bacteria direct T cells to adopt distinct functions remains poorly understood. Here, we investigated which cells and molecular components are required for iTreg cell differentiation. We found that antigen presentation by cells expressing RORγt, rather than by classical dendritic cells, was required and sufficient for iTreg induction. These RORγt^{+} cells, likely type 3 innate lymphoid cells and/or recently-described Janus cells[5], require antigen presentation machinery, the chemokine receptor CCR7, and TGF-β activator α_v integrin. In the absence of any of these, instead of iTreg there was expansion of pathogenic Th17 cells, induced by CCR7-independent antigen presenting cells (APCs). Thus, intestinal commensal microbes and their products target multiple APCs with pre-determined features suited to directing appropriate T cell differentiation programs, rather than a common APC that they endow with appropriate functions.

A subset of bacterial species among the hundreds that comprise the gut microbiota elicit stereotypic antigen-specific T cell differentiation programs through mechanisms yet to be elucidated. It is generally accepted that conventional (or classical) dendritic cells (cDC) that migrate from tissue to the inductive sites in lymph nodes present microbial antigens to activate and promote differentiation of naive antigen-specific T cells[4,6–10]. However, the antigen presenting cells (APCs) that execute these functions according to instructions of distinct intestinal bacterial species have not been clearly defined. We have chosen to study the APC requirements for T cell responses to *H. hepaticus* (Hh), which elicits iTreg, Tfh, or pathogenic Th17 cells under different conditions[3].

Distinct APCs program gut CD4^{+} T cells

To study the properties of antigen-presenting cells that direct the differentiation of microbiota-specific iTreg cells, we transferred into Hh-colonized mice naive Hh-specific CD4^{+} T cells from HH7–2 TCR transgenic mice[3]. CFSE-labeled transferred T cells exhibited robust proliferation by day 3 in colon-draining C1 mesenteric lymph nodes

(MLN) of wild type (WT) mice, with up-regulation of Foxp3 and RORγt, characteristic of colonic iTreg cells[11,12]. In contrast, in mice deficient for antigen presentation by DC (and, potentially, other cells: *CD11c-Cre;I-Ab^f/f*, designated as *MHCII ^CD11c*), there was no expression of Foxp3 by the Hh-specific T cells, but, surprisingly, there was substantial proliferation of these cells, with up-regulation of RORγt (Fig. 1a). At 2–3 weeks after transfer, there was expansion in the colonic lamina propria of RORγt- and T-bet-expressing Hh-specific T cells in mutant mice, characteristic of a pro-inflammatory program (Extended Data Fig. 1a–c). Endogenous T cells also displayed this phenotype, with fewer Foxp3+ RORγt+ iTreg and expansion of Th17 cells (Extended Data Fig. 1b). This result suggested that antigen presentation by *Cd11c*-lineage cells is required for iTreg cell differentiation, but that it is dispensable for the differentiation of pro-inflammatory Th17 cells.

The chemokine receptor CCR7 mediates migration of DC and T cells into lymph nodes, where adaptive immune responses are initiated, and is critical for tolerogenic responses to food antigens[13]. In CCR7-deficient mice, iTreg induction in response to Hh colonization failed (Extended Data Fig. 1d), in agreement with the recent demonstration of a CCR7 requirement for the differentiation of iTreg cells specific for other *Helicobacter* species[6]. However, we observed robust priming and proliferation of RORγt+ Hh-specific T cells in CCR7-deficient mice (Extended Data Fig. 1d). In *CD11c-Cre;Ccr7^f/f* conditional mutant mice[14] (designated *Ccr7 ^CD11c*), transferred Hh-specific T cells failed to differentiate into iTreg cells, despite exhibiting robust proliferation, as in CCR7-deficient mice (Fig. 1b). In the colon of these mice, *Hh*-specific iTreg cells were rare, but there was accumulation of inflammatory Th17 cells along with elongation of the crypts (Fig. 1c, Extended Data Fig. 1e,f). Together, our results indicate that, unlike iTreg, microbiota-specific inflammatory Th17 cell differentiation does not depend on either CCR7 or antigen presentation by CD11c-expressing cells.

Antigen presentation for iTreg induction

Classical DC, which have been broadly divided into cDC1 and cDC2, comprise multiple cell subsets that differ in their ontogeny, location, and transcription factor dependency[15,16]. Both cDC1 and cDC2 have been proposed to initiate iTreg responses, largely based on their ability to induce Treg cell differentiation *in vitro*[9,17]. However, *in vivo* depletion of cDC1 or cDC2 failed to phenocopy iTreg loss (Extended Data Fig. 1g–i), in agreement with previous reports[6,18–20]. These findings suggested that antigen presentation by a rare uncharacterized *Cd11c*-lineage myeloid or non-myeloid cell subset is required for iTreg cell differentiation. To identify putative antigen presenting cell populations targeted by *CD11c-cre*, we performed CITE-seq analysis of cells isolated from MLN of Hh-colonized *CD11c-Cre;ROSA26LSLtdTomato* (designated *tdTomato-ON ^CD11c*) fate-map mice (Fig. 2a and Extended Data Fig. 2a,b). In addition to expected myeloid cell subsets, we identified both type 3 innate lymphoid cells (ILC3) and a recently described Aire+ RORγt+ population, named Janus cells (JC)[5,21], among the tdTomato+ cells, and these also expressed MHCII (Fig. 2b and Extended Data Fig. 2b). Using a gating strategy for JC (Extended Data Fig. 3a–d), we confirmed that they, like ILC3, express *Rorc* (Extended Data Fig. 2a). Consistent with this, GFP+ ILC3 and JC from the C1 MLN of *RORγt-eGFP* mice expressed both CD11c and CD11b or mostly CD11c, respectively, and were both targeted by *CD11c-Cre*

(Fig. 2c, Extended Data Fig. 2b and 3e). Accordingly, many fewer RORγt^{+} cells from MLN of *MHCII* [CD11c] mice expressed MHCII, as compared to WT littermates (Extended Data Fig. 4a).

Expression of MHCII by ILC3 was reported to prevent microbiota-dependent expansion of inflammatory T cells in the intestine, and was proposed to mediate negative selection of those cells[22]. Our results suggested that *CD11c-Cre*-expressing RORγt^{+} cells may, instead, be required for the differentiation of microbiota-specific iTreg cells. This was confirmed by examining iTreg cell differentiation in mice whose MHCII was inactivated in presumptive ILC3 and JC (*RORγt-Cre;I-AB[l/l]*, designated as *MHCII* [RORγt]). Despite expression of MHCII in cDC2 of these mutant mice (Fig. 2d), there was complete loss of Hh-specific iTreg cell differentiation in colon-draining MLN, but intact priming and subsequent expansion of pathogenic Th17 cells in the large intestine lamina propria (Fig. 2e,f, Extended Data Fig. 4b). Both the donor Hh-specific and host T cells exhibited loss of iTreg and increase in IFNγ- and IL-17A-producing CD4^{+} T cells in the large intestine lamina propria (Fig. 2f, Extended Data Fig. 4c–e). Similar results were observed with Hh-specific T cells in another conditional mutant strain, *RORγt-Cre; H2-DMa[f/f]* mice (*H2-DMa* [RORγt]) deficient in H2-DMa, the mouse equivalent of HLA-DM, required for displacement of invariant chain peptide and loading of processed peptide on MHCII molecules[23]. This result confirms that the antigen processing machinery is required in RORγt[+] APCs for induction of microbiota-specific iTregs (Extended Data Fig. 4f).

RORγt[+] APCs require CCR7 for iTreg induction

Intestinal ILC3 have been reported to also employ CCR7 for migration to draining MLN[24,25]. We found expression of *Ccr7* in both ILC3 and JC (Extended Data Fig. 2a and 5a). We therefore asked whether CCR7 is required for migration of RORγt [+] APCs rather than classical DC for iTreg induction. Indeed, Hh-specific iTreg cell differentiation was abrogated in the MLN of *Ccr7* [RORγt] mice (Fig. 3a). In the colon of *Ccr7* [RORγt] mutant mice, there was skewing of Hh-specific T cells towards a Th1-Th17 inflammatory program after 2–3 weeks of adoptive T cell transfer, although this was less marked than in *Ccr7* [CD11c] mice, and elongation of crypts was not observed (Fig. 3b and data not shown). To determine whether loss of CCR7 affects migration of RORγt^{+} cells to the MLN, we reconstituted irradiated mice with equal numbers of WT and *RORγt-Cre;Ccr7[f/f]* (*Ccr7* [RORγt]) bone marrow cells. Although there was no effect on the ratio of WT and mutant migratory DC, there was a substantial reduction in the proportion of CCR7-deficient lymphoid tissue inducer (LTi)-like ILC3, but no significant difference in the proportions of other RORγt^{+} cells in the MLN (Fig 3c and Extended Data Fig. 5b–d). Similarly, in *Ccr7* [CD11c] mice, LTi-like ILC3 lost CCR7 expression and were reduced in number in the MLN (Extended Data Fig. 5e,f). Although JC numbers in the MLN did not appear to be affected by loss of CCR7, the chemokine receptor may be required for migration of the cells within the lymph node, localizing them for appropriate antigen presentation. To further study a potential role for JC, we examined the T cell response to Hh in *RORγt-cre;Aire[f/f]* mice and in Aire-DTR bone marrow-reconstituted mice treated with diphtheria toxin. In neither case was there an effect on Hh-specific iTreg cell differentiation (Extended Data Fig. 5g–h). We cannot, however, rule out a role for JC, as Aire may not be required for the microbiota-

dependent iTreg inductive function of these cells and residual cells in DT-treated animals may be sufficient to support iTreg cell differentiation. Together, these results indicate that RORγt+ APCs, either LTi-like ILC3 or JC, migrate to or within the MLN, where they present microbial antigen to naïve T cells to induce iTreg cell differentiation, and that their failure to migrate results, instead, in inflammatory Th17 cell differentiation.

Role of integrins in iTreg differentiation

Differentiation of iTreg cells requires TGF-β signaling in CD4+ T cells, and defects in this pathway result in spontaneous colitis[3,11]. TGF-β is released from its latent form on cell surfaces or extracellular matrix following physical interaction with integrins $\alpha_v\beta_6$ or $\alpha_v\beta_8$[26–28]. Loss of integrins β_8 or α_v in hematopoietic cells, including in *CD11c-Cre:Itgb8$^{f/f}$* mice, resulted in reduced colonic Tregs and in multiorgan inflammation[29–31]. Consistent with those observations, differentiation of adoptively transferred Hh-specific T cells into iTreg cells was abrogated both following treatment of mice with anti-β_8 antibody and in *CD11c-Cre;Itgav$^{f/f}$* (Itgav ^{CD11c}) recipient mice (Fig. 4a,b). We examined iTreg cell differentiation in mice with conditional inactivation of *Itgav* in RORγt+ APCs and in T cells (*Itgav^{RORγt}*) (Fig. 4c,d). In the colon-draining MLN of *Itgav^{RORγ}* mice, there was loss of integrin α_v (CD51) expression on both ILC3 and JC, and adoptively transferred Hh-specific T cells failed to express Foxp3 (Fig. 4c and Extended Data Fig. 6a). The MLN were increased in size (Extended Data Fig. 6b) and the Hh-specific T cells expressed RORγt, but, unlike in control littermates, they also had elevated T-bet, along with a substantial decrease in CCR6, consistent with reduced TGF-β signaling (Extended Data Fig. 6c). Notably, β_8 antibody blockade resulted in the same phenotype (Extended Data Fig. 6d). In the colonic lamina propria of *Itgav^{RORγt}* mice, there was loss of both Hh-specific and host-derived iTreg cells, with skewing of CD4+ T cells towards IFNγ+ Th1 and pathogenic Th17 programs (Fig. 4d, Extended Data Fig. 6e), suggesting that expression of integrin α_v on RORγt+ APCs, likely in partnership with integrin β_8, is a general requirement for intestinal iTreg cell differentiation. Although ILC3 express higher levels of CD51 (Extended Data Fig. 6a), single-cell RNA sequencing analysis of GFP+ cells from pooled lymph nodes of *Aire* reporter mice[32] showed clustering of JCs into three discrete subpopulations, with JC2 and JC3 expressing high levels of *Itgav* and *Itgb8* (Extended Data Fig.7a–e). JC and a fraction of ILC3, obtained from *Itgb8-IRES-tdTomato* reporter mice[33], were found to express tdTomato (Extended Data Fig 7f–g), and we therefore cannot exclude the requirement of either cell type for iTreg differentiation. Differentiation of iTreg cells was normal in *CD4-Cre;Itgav$^{f/f}$* mice (Extended Data Fig. 6f), consistent with a role of the integrin in RORγt+ APCs rather than in TCRαβ T cells. Furthermore, we reconstituted mice after irradiation with a mix of MHCII ^{CD11c} and *Itgav^{RORγt}* bone marrow cells, resulting in binary expression of MHCII or integrin α_v. In these mice, iTreg cell differentiation was abolished, consistent with a requirement for both antigen presentation and activation of TGF-β by the same APC, coupling T cell activation with differentiation cues (Fig. 4e–f, Extended Data Fig. 6g).

Tregs and sufficiency for RORγt+ APCs

Our results support a role for *RORγt+* APCs in microbiota-specific iTreg differentiation, but do not rule out a requirement for additional conventional antigen presenting cells. Moreover,

a population of DC (T-bet-negative cDC2) was recently reported to express RORγt[34], raising the possibility that neither ILC3 nor JC is relevant in iTreg cell differentiation. To examine a potential role for a rare DC subset, we employed *zbtb46-Cre*, considered to specifically target cDC, and *zbtb46* reporter mice. Because *zbtb46-Cre;Ccr7^f/-* mice (CCR7 ^zbtb46) were unable to support microbiota-dependent iTreg cell differentiation (Extended Data Fig. 8a), we profiled by CITE-seq sorted cells from C1 mLN of *zbtb46-eGFP ; RORγt-Cre;ROSA26LSLtdTomato* (*tdTomato-ON^RORγt*) mice, expressing one or both fluorescent reporters, gated to exclude B and T cells (Extended Data Fig. 8b). Surprisingly, GFP expression was identified on all ILC3 and fate-mapped JC. Zbtb46 expression on ILC3 was confirmed using *mKate2-ON^zbtb46; RORγt-eGFP* mice (Extended Data Fig. 8c). We identified a few migratory cDC2 among tdTomato^+ GFP^+ cells in *zbtb46-eGFP; tdTomato-ON^RORγt* mice, but these did not form a subcluster to suggest a unique gene signature and did not exhibit active *Rorc* or integrin α_v mRNA and protein expression (Extended Data Fig. 8d–f), suggesting that they are unlikely to be RORγt^+ APCs required to direct iTreg cell differentiation. We performed three-dimensional intravital imaging studies to visualize interactions of newly-primed Hh-specific T cells with DC and *RORγt^+* APCs populations in C1 MLN. We utilized *mKate2-ON^zbtb46; RORγt-eGFP* mice to visualize cDC (mKate2^+) and *RORγt^+* APCs (eGFP^+ and mKate2). However, given that the efficiency of *zbtb46-Cre*-mediated activation of the mKate2 reporter was low (~20% for *RORγt+* APCs and cDC populations) (Extended Data Fig. 8g), we additionally utilized cell morphology and size analysis to distinguish the few host-derived GFP^+ T cells from GFP^+ *RORγt^+* APCs. We next transferred dye-labeled *Nur77-eGFP* Hh-specific T cells into these fluorescent reporter host mice to measure direct interactions of primed T cells (which up-regulate *Nur77*) with DC and *RORγt^+* APCs at 15 h after adoptive transfer. Approximately 81% of GFP^+ primed Hh-specific T cells were found in contact with at least one *RORγt^+* APC with/without DC, as opposed to only ~31% of the non-primed T cells (Extended Data Fig. 8h,i).

Our imaging study and results with conditional mutant mice did not rule out a contribution by DC towards Hh-specific T cell activation and iTreg differentiation. We therefore wished to determine whether antigen presentation limited to only *RORγt-Cre*-expressing cells was sufficient to allow for iTreg cell differentiation. For this purpose, we used mice that express MHCII only in *RORγt^+* APCs, and not in DC or other APCs (*RORγt-Cre;I-AB^-/Δsl* , designated *MHCII-ON^RORγt*). We reconstituted irradiated congenic mice with bone marrow from *MHCII ^CD11c* mice with or without bone marrow from WT or *MHCII-ON^RORγt* mice (Fig. 5a). Flow cytometry analysis confirmed MHCII expression by *RORγt^+* cells, but not DC from the C1 MLN and the colon lamina propria of *MHCII ^CD11c;MHCII-ON^RORγt* bone marrow-reconstituted mice (Fig. 5b, Extended Data Fig. 9a). As expected, in control mice reconstituted with only *MHCII ^CD11c* bone marrow cells, in which no MHCII expression was detected in either *RORγt^+* APCs or DC, there was no differentiation of adoptively transferred Hh-specific iTreg cells, but there was, instead, differentiation of RORγt^+Tbet^+ inflammatory Th17 cells (Fig. 5c,d). In contrast, antigen presentation by RORγt^+ cells alone was sufficient to rescue iTreg cell differentiation and suppression of inflammatory T cells in response to Hh colonization, as seen in mice reconstituted with *MHCII ^CD11c* plus *MHCII-ON^RORγt* bone marrow cells (Fig. 5c,d), or with only *MHCII-*

$ON^{ROR\gamma t}$ cells (Extended Data Fig. 9c). There was similar rescue of endogenous iTreg cell differentiation in mice having the gain-of-function MHCII in $ROR\gamma t^+$ cells (Extended Data Fig. 9b). It should be noted that whereas there was rescue of Hh-directed iTreg cell differentiation in mice reconstituted with $MHCII\text{-}ON^{ROR\gamma t}$ bone marrow, there was a marked absence of Bcl6-expressing Tfh cells, which are also induced by Hh (Fig. 5c,d; Extended Data Fig. 9c). Interestingly, Tfh cells were present in mice reconstituted with only $MHCII\text{-}ON^{CD11c}$ bone marrow, suggesting that their differentiation requires antigen presentation by DC and/or B cells, as proposed previously[35] (Extended Data Fig. 9c). We conclude that $ROR\gamma t^+$ APCs, ILC3 and/or JC, are specialized to prime naive microbiota-specific T cells and guide their differentiation into iTregs, but other APCs are required to guide the differentiation of microbiota-specific pathogenic Th17 cells and Tfh cells.

Discussion

The composition of the intestinal microbiota influences host immune functions that contribute to anti-microbial host defense, inflammatory disease, and anti-tumor immunity. Transmission of information from gut microbes to immune system cells remains poorly understood. The current results indicate that $ROR\gamma t^+$ cells, either JC, whose transcriptional profile suggests a role in promoting immunological tolerance[5], or type 3 innate lymphoid cells previously implicated in restraining microbiota-dependent Th1/Th17 inflammatory responses in the gut[36,37], do so in large part by conveying signals from the microbiota to naive bacteria-specific T cells, activating them and guiding their differentiation towards a unique iTreg cell program. $ROR\gamma t^+$ cells defective for CCR7-mediated migration (either to or within the MLN), MHCII antigen presentation, or $\alpha v \beta 8$ function (presumably through activation of TGF-β), failed to induce the iTreg program. Intriguingly, under such circumstances there was expansion of pathogenic Th17 cells that promoted intestinal inflammation. We previously demonstrated that a T cell-intrinsic c-Maf deficiency prevented iTreg cell differentiation, and similarly allowed for microbiota-dependent differentiation of pathogenic Th17 cells[3]. Together, these findings suggest that iTreg cells restrain the priming, proliferation, and differentiation of Th17 cells in the MLN. The APC(s) that directs pathogenic Th17 cell differentiation does not require CCR7, and it is not targeted in CD11c-Cre mice, and is, therefore, most likely not a cDC, but its identity is currently not known. One hypothesis is that iTreg cells might not only inhibit Th17 cell differentiation and function but also may inhibit the function of the CCR7-independent Th17 inducer APC (Extended Data Fig. 10).

It has been proposed that intrinsically different APC subsets direct distinct T cell responses[38], but such processes have been difficult to demonstrate in the setting of immune responses *in vivo*. Our study shows that a unique $ROR\gamma t^+$ cell type instructs naïve microbiota-specific CD4$^+$ T cells to become iTreg cells, but does not support the differentiation of other T cell programs, including Tfh cells, that are normally also induced by Hh intestinal colonization. Although our results are most compatible with the $ROR\gamma t^+$ APC being an ILC3 or Aire$^+$ JC subset, we cannot rule out that it may represent a novel $ROR\gamma t^+$ cell type that cannot yet be categorized as either lymphoid or DC-like. Definitive identification and characterization of this cell awaits more specific genetic tools than those currently available. Nevertheless, our results clearly demonstrate the existence of multiple

APCs that are targeted by a specific commensal microbe to instruct diverse effector T cell functions (Extended Data Fig. 10). The APCs may act hierarchically, as exemplified here by RORγt+ cells that supersede the function of Th17-inducing APCs. The existence and identity of distinct cellular circuits responsible for the induction of iTregs and other T cell functional subsets offers the opportunity to investigate the corresponding cells in humans and, potentially, to modulate them therapeutically.

Methods

Mice

Mice were bred and maintained in the Alexandria Center for the Life Sciences animal facility of the New York University School of Medicine, in specific pathogen-free conditions. C57BL/6 mice (Jax# 000664), *Batf3*^{−/−} (*B6.129S(C)-Batf3tm1Kmm/J* #Jax 013755), *Itgav^{f/f}* (*B6.129P2(Cg)-Itgav^{tm2Hyn}/J* Jax# 032297, CD45.1 mice (*B6.SJL-Ptprca Pepcb/BoyJ*, Jax# 002014), *CD4-Cre* (*Tg(Cd4-cre)1Cwi/BfluJ*, Jax# 017336), *CD11c-Cre* (*B6.Cg-Tg(Itgax-cre)1–1Reiz/J* #Jax 008068), *Ccr7*^{−/−} (*B6.129P2(C)-Ccr7tm1Rfor/J*, Jax# 006621), *I-AB^{f/f}* (*B6.129X1-H2-Ab1tm1Koni/J* #Jax 013181), *Zbtb46-Cre* (*B6.Cg-Zbtb46tm3.1(cre)Mnz/J* #Jax 028538), *Zbtb46-eGFP* (*B6.129S6(C)-Zbtb46tm1.1Kmm/J* #Jax 027618), tdTomato^{LSL} (*B6;129S6-Gt(ROSA)26Sortm14(CAG-tdTomato)Hze/J* #Jax 007908), *Aire^{f/f}* (*B6.Cg-Airetm1Dfil/J* #Jax 031409), *Nur77-eGFP* (*C57BL/6-Tg(Nr4a1-EGFP/cre)820Khog/J* #Jax 016617), CD90.1 (*B6.PL-Thy1a/CyJ* #Jax 000406) mice were purchased from Jackson Laboratories. RORγt-Cre and Hh7-2tg were generated in our laboratory and previously described[3,39]. BAC-transgenic Rorc(t)-GfpTG were generated by G. Eberl's lab[40]. *huLangerin (CD207)-DTA* mice were kindky provided by Daniel H. Kaplan[41]. Ccr7^{f/f} mice were previously described[14]. *mKate2^{LSL}* mice[42] were provided by Scott Lowe. I-AB lox-STOP-lox[35], Aire-DTR[43], H2-DMa1^{f/f}[23], *Itgb8-IRES-tdTomato*[33] and Adig (Aire-Driven Igrp-Gfp)[32] mice have been described. Littermates with matched sex (both males and females) were used. Mice in all the experiments were 6–12 weeks old at the starting point of treatment. Animal sample size estimates were determined using power analysis (power=90% and alpha=0.05) based on the mean and standard deviation from our previous studies and/or pilot studies using 4–5 animals per group. All animal procedures were performed in accordance with protocols approved by the Institutional Animal Care and Usage Committee of New York University School of Medicine.

Commercialized antibodies, intracellular staining and flow cytometry

The following monoclonal antibodies were purchased from eBiosciences, BD Pharmingen or BioLegend:

CD3 biotinylated (145-2C11), Tonbo Bio 30-0031-U500, 1:100;CD3 TotalSeq™-A0182 (17A2),BioLegend 100251, 1:100;CD4 AF700(RM4-5), Thermo Scientific 56-0042-82, 1:400;CD4 BUV395(GK1.5), BD 563790, 1:400;CD25 APC (PC61), Thermo Scientific 17-0251-82, 1:200;CD25 TotalSeq™-A0097 (PC61), BioLegend 102055, 1:100;CD25 BV421 (PC61), BioLegend 102033, 1:200;CD25 PE (PC61), Invitrogen 12-0251-83, 1:200;CD44 PerCP-Cyanine5.5 (IM7), Thermo Scientific 45–0441-82, 1:400;CD44 AF700 (IM7), BD 560567, 1:200;CD45.1 BV650(A20), BD563754, 1:400;CD45.1 BV421(A20),

BD 563983, 1:200;CD45.2 AF594 (104), BioLegend 109850, 1:200;CD45.2 FITC (104), eBioscience 11–0454-85, 1:400;CD90.1 APC-e780(HIS51), Thermo Scientific 47–0900-82, 1:400;CD90.2 PerCP-Cyanine5.5 (53-2.1), BioLegend 140316, 1:200;CD90.2 FITC (30-H12), BD 553013, 1:400;CD90.2 APC e780 (53–2.1), eBioscience 47–0902-82, 1:200;CD90.2 TotalSeq™-A0075 anti-mouse (30-H12), BioLegend 105345, 1:100;CD19 PerCP-Cyanine5.5 (1D3), Tonbo Bioscience 65–0193-U100, 1:400;CD45R/B220 PerCP-Cyanine5.5 (RA3–6B2), Invitrogen 45-0452-82, 1:400;CD45R/B220 BV510 (RA3–6B2), BD B563103, 1:400;CD45R/B220 biotinylated (RA3–6B2), Thermo Fisher 13-0452-85, 1:100;CD45R/B220 BV785 (RA3–6B2), BioLegend 103246, 1:200;CD127 PE (A7R34), eBioscience 12-1271-83, 1:100;CD127 BV650 (A7R34), BioLegend 135043, 1:100;CD127 PerCP-Cyanine5.5 (A7R34), BioLegend 135021, 1:50;CD127 (IL-7Rα) TotalSeq™-A0198 (A7R34), BioLegend 135045, 1:100;CD51 PE (RMV-7), BioLegend 104106, 1:100;CD51 BUV395 (RMV-7), BD 747834, 1:100;CD51 TotalSeq™-A1008 (RMV-7), BioLegend 104111, 1:100;MHCII I-A/I-E AF700 (56-5321-82), eBioscience 56-5321-80, 1:200;MHCII I-A/I-E BV421 (M5/114.15.2), BioLegend 107631, 1:400;CCR6 BV711(140706), BD 740646, 1:400;CCR6 BV421(29-2L17), Biolegend 129817, 1:150;CCR6 BUV395(140706), BD 747831, 1:50;CCR6 TotalSeq™-A0225 (29-2L17), BioLegend 129825, 1:100;NKp46 AF467 (29A1.4), BioLegend 137628, 1:200;NK1.1 PerCP-Cyanine5.5 (PK136), Invitrogen 45-5941-82, 1:200;CD62L APC (MEL-14), Fisher Scientific 50-150-09, 1:400;CXCR5 APC (L138D7), BioLegend 145506, 1:200;CXCR5 TotalSeq™-A0846 (L138D7), BioLegend 145535, 1:100;TCRβ BV711 (H57-597), BD 563135, 1:200;TCRβ APC e780 (H57-597), Invitrogen 47-5961-82, 1:200;TCRβ BV510 (H57-597), BD 563221, 1:200;TCRβ biotinylated (H57-597), Thermo Fisher 13-5961-85, 1:100;TCRβ FITC (H57-597), BioLegend 109206, 1:200;TCRg/d BV510 (GL3), BioLegend 118131, 1:200;TCRg/d FITC (GL3), BioLegend, 118105, 1:200;TCRg/d PerCP-Cyanine5.5 (GL3), BioLegend 118117, 1:400;TCR Vβ6 PerCP-eFluor 710, (RR4-7), Thermo Scientific 46-5795-82, 1:400;TCR Vβ6 FITC (RR4-7), BD 553193, 1:400;Bcl-6 BV421 (K112-91), BD 563363, 1:50;Foxp3 PE-Cy7 (FJK-16s), eBioscience 25-5773-82, 1:200;Foxp3 e660 (FJK-16s), Thermo Scientific 50-5773-82, 1:200;RORγt BV421 (Q31-378), BD 562894, 1:200;RORγt PE (B2D), Thermo Scientific 12-6981-82, 1:200;T-bet PE-CF594 (O4–46), BD 562467, 1:70;IL-17A AF700 (TC11-18H10.1) BioLegend 506914, 1:200;IFN-γ PE-Cy7 (XMG1.2), BioLegend 505826, 1:200;CD11c PE-Cy7 (N418), BioLegend 117318, 1:400;CD11c BV711 (HL3), BD 563048, 1:100;CD11c TotalSeq™-A0106 (N418), BioLegend 117355, 1:100;CD11b BUV395 (M1/70), BD 563553, 1:400;CD11b APC-e780 (M1/70), Invitrogen 47-0112-82, 1:400;CX3CR1 PE (SA011F11), BioLegend 149006, 1:200;CX3CR1 TotalSeq™-A0563 (SA011F11), Biolegend 149041, 1:100;Ly6c PerCP (HK1.4), BioLegend 128028, 1:200;SIRPa FITC (P84), BioLegend 144006, 1:400;Ly6G PerCP-Cyanine5.5 (1A8), BioLegend 127616, 1:400;CD273 APC (TY25), BioLegend 107210, 1:100; Clec12a PE (5D3), BD 562773, 1:200;CD103 BV421 (M290), BD 562771, 1:100;CD103 PE/dazzle 594 (2E7), Biolegend 121430, 1:200;XCR1 APC Cy7 (ZET), Biolegend 148224, 1:200;CCR7 PE(4B12), BD 560682, 1:100;CCR7 BV421(4B12), BioLegend 120119, 1:100;CXCR6 PE/dazzle 594 (SA051D1), biolegend 151117, 1:200;CXCR6 APC (DANID2), Thermo Scientific ebioscience 17-9186-82, 1:400;CXCR6 PE-Cy7 (SA051D1), biolegend 151118, 1:200;CD40 biotinylated (HM40-3), eBioscience, 1:100;CD40 biotinylated (3/23), BioLegend 124606, 1:100;TER-119

(TER-119) biotinylated, Thermo Fisher 13-5921-85, 1:200;CD16/32 (2.4G2), Bio X Cell BE0307, 1:400;CD64 TotalSeq™-A0202 (X54-5/7.1), BioLegend 139325, 1:100;CD14 TotalSeq™-A0424 (Sa14-2), BioLegend 123333, 1:100;CD115 TotalSeq™-A0105 (AFS98), BioLegend 135533, 1:100;Ly-6G/Ly-6C TotalSeq™-A0116 (RB6-8C5), BioLegend 10845910, 1:100;CD192 (CCR2) TotalSeq™-A0426 (SA203G11), BioLegend 150625, 1:100;TotalSeq™-A0301 anti-mouse Hashtag 1 Antibody (M1/42; 30-F11), BioLegend 155801 , 1:100;TotalSeq™-A0302 anti-mouse Hashtag 2 Antibody (M1/42; 30-F11) BioLegend 155803, 1:100;TotalSeq™-A0303 anti-mouse Hashtag 3 Antibody (M1/42; 30-F11) BioLegend 155805, 1:100;TotalSeq™-A0304 anti-mouse Hashtag 4 Antibody (M1/42; 30-F11) BioLegend 155807, 1:100;TotalSeq™-A0305 anti-mouse Hashtag 5 Antibody (M1/42; 30-F11) BioLegend 155809, 1:100;TotalSeq™-A0306 anti-mouse Hashtag 6 Antibody (M1/42; 30-F11) BioLegend 155811, 1:100;TotalSeq™-A0307 anti-mouse Hashtag 7 Antibody (M1/42; 30-F11) BioLegend 155813, 1:100;TotalSeq™-A0308 anti-mouse Hashtag 8 Antibody (M1/42; 30-F11) BioLegend 155815, 1:100; streptavidin BV650, BD 563855, 1:400; 4′,6-diamidino-2-phenylindole (DAPI) or Live/dead fixable blue (ThermoFisher) was used to exclude dead cells.

For transcription factor staining, cells were stained for surface markers, followed by fixation and permeabilization before nuclear factor staining according to the manufacturer's protocol (Foxp3 staining buffer set from eBioscience). For cytokine analysis, cells were incubated for 5 h in RPMI with 10% FBS, phorbol 12-myristate 13-acetate (PMA) (50 ng/ml; Sigma), ionomycin (500 ng/ml; Sigma) and GolgiStop (BD). Cells were stained for surface markers before fixation and permeabilization, and then subjected to intracellular cytokine staining according to the manufacturer's protocol (Cytofix/Cytoperm buffer set from BD Biosciences). Flow cytometric analysis was performed on an LSR II (BD Biosciences) or an Aria II (BD Biosciences) with BD FACSDiva™, or Cytek Aurora (Cytek) using SpectroFlo (v3.03) and analyzed using FlowJo 10.8.1 software (Tree Star).

Flow cytometry gating strategy

Hh7-2 gating: FSC, SSC; Live Dead⁻,singlets, Dump⁻ (B220,TCRgd, Ly6G), MHCII⁻, CD4⁺, TCRβ⁺, VB6⁺, CD45.1⁺ or CD90.1⁺; **cDC gating**: FSC, SSC; Live Dead⁻,singlets, Dump⁻ (B220, TCRβ, TCRgd, Ly6G), CD11c⁺ and CD11b⁺ , SIRPa$^{low-moderate}$ (remove CD11c⁻, SIRPA^{high}); **cDC2 gating** (unless mentioned otherwise): FSC, SSC; Live Dead⁻,singlets, Dump⁻ (B220,TCRgd, Ly6G), CD11c⁺ and CD11b⁺ , SIRPa$^{low-moderate}$ (remove CD11c⁻, SIRPA^{high}), Clec12a⁻ SIRPa⁺; **migratory cDC2 gating**: FSC, SSC; Live Dead⁻,singlets, Dump⁻ (B220,TCRgd, Ly6G), CD11c⁺ and CD11b⁺ , SIRPa$^{low-moderate}$ (remove CD11c⁻, SIRPA^{high}), Clec12a⁻ SIRPa⁺, PDL2⁺; **NCR1⁺ ILC3 gating**: FSC, SSC; Live Dead⁻,singlets, Dump⁻ (B220,TCRgd, Ly6G), TCRβ⁻ , CD90+, Il7R⁺, RORγt⁺, CCR6⁻, NCR1⁺; **JC** (using internal staining): FSC, SSC; Live Dead⁻,singlets, Dump⁻ (B220,TCRgd, Ly6G), TCRβ⁻ , RORγt⁺, MHCII+ CXCR6⁻, Il7R⁻; **JC** (excluding internal staining): FSC, SSC; Live Dead⁻,singlets, Dump⁻ (B220,TCRgd, Ly6G), TCRβ⁻ , CD11c$^{low-negative}$, MHCII⁺, CCR6⁺,CXCR6⁻, Il7R⁻ ; **ILC3**: FSC, SSC; Live Dead⁻,singlets, Dump⁻ (B220,TCRgd, Ly6G), TCRβ⁻ , CXCR6⁺, Il7R⁺, RORγt⁺; **LTi-Like ILC3** (using internal staining): FSC, SSC; Live Dead⁻,singlets, Dump⁻ (B220,TCRgd, Ly6G), TCRβ⁻ , MHCII+, CXCR6⁺, Il7R⁺, RORγt⁺, CCR6⁺, CD25⁺; **LTi-Like ILC3**

(excluding internal staining): FSC, SSC; Live Dead⁻,singlets, Dump⁻ (B220,TCRgd, Ly6G), TCRβ⁻ , CD11c^low-negative, MHCII⁺, CCR6⁺,CXCR6⁺, Il7R⁺

Isolation of lymphocytes and APCs

After removal of caecal patches, large intestine tissues were sequentially treated with PBS containing 1 mM DTT at room temperature for 10 min, twice with 5 mM EDTA at 37 °C for 10 min to remove epithelial cells, and then minced and dissociated in digestion buffer (RPMI containing collagenase (1 mg ml−1 collagenase D; Roche), DNase I (100 μg ml−1; Sigma), dispase (0.1 U ml−1; Worthington) and 10% FBS) with constant stirring at 37 °C 55 min. Leukocytes were collected at the interface of a 40%/80% Percoll gradient (GE Healthcare). Lymph nodes were mechanically disrupted for lymphocyte isolation. For isolation of myeloid cells and ILC, lymph nodes were mechanically disrupted with digestion buffer with constant stirring at 37 °C 30 min.

H. hepaticus culture and oral infection

H. hepaticus was kindly provided by Dr. James Fox (MIT). Hh was cultured and administrated as was previously described[3]. Frozen stock aliquots of *H. hepaticus* were stored in Brucella broth with 20% glycerol and frozen at −80°C. The bacteria were grown on blood agar plates (TSA with 5% sheep blood, Thermo Fisher). Inoculated plates were placed into a hypoxia chamber (Billups-Rothenberg), and anaerobic gas mixture consisting of 80% nitrogen, 10% hydrogen, and 10% carbon dioxide (Airgas) was added to create a micro-aerobic atmosphere, in which the oxygen concentration was 3~5%. The micro-aerobic jars containing bacterial plates were left at 37°C for 4 days before animal inoculation. For oral infection, *H. hepaticus* was resuspended in Brucella broth by application of a pre-moistened sterile cotton swab applicator tip to the colony surface. 0.3 mL bacterial suspension was administered to each mouse by oral gavage. Mice were inoculated for a second dose after 3 days.

Adoptive transfer of Hh7-2 TCR transgenic cells

Adoptive transfer of Hh7-2 was done as was previously described[3], with minor modifications. Recipient mice were colonized with *H. hepaticus* by oral gavage seven days before adoptive transfer. Spleens and lymph nodes from donor Hh7-2 TCRtg mice were collected and mechanically disassociated. Red blood cells were lysed using ACK lysis buffer (Lonza). Naive Hh7-2 T cells were sorted as CD4⁺TCRβ⁺CD44^lo CD62L^hi CD25⁻Vβ6⁺ (HH7-2tg), on the Aria II (BD Biosciences). For analysis of early differentiation, cells were additionally labeled with CFSE (ThermoFisher). Cells were resuspended in PBS on ice and 100K were transferred into congenic isotype-labelled recipient mice by retro-orbital injection. Cells from MLN were analyzed 3 days after transfer and cells from colon LP were analyzed 10–14 days after transfer.

CITE-seq

CITE-seq and cell hashing were performed as described[44,45] with minor modifications. Single-cell suspensions were obtained from digests of C1 MLN of t*dTomato-ON*^CD11c or *tdTomato-ON*^RORγt *; zbtb46-eGFP* mice that had been colonized with *Helicobacter*

for 7 days. Cells were sorted on a BD FACSAriaII using a 100-μm nozzle. Dead cells as well as T cells and B cells were gated out using DAPI, TCRβ, TCRγδ and B220 antibodies. From t*dTomato-ON*[CD11c] mice, the tdTomato+ population was collected separately from two mice. From *tdTomato-ON*[RORγt] *; zbtb46-eGFP* mice, we collected 3 populations from two separate mice: GFP[+], GFP[+] tdTomato[+] and tdTomato[+]. Sorted cells were stained separately with hashing antibodies (Biolegend)[45]. After removal of excess hashing antibodies, we combined the samples and stained them with CITE-seq antibodies, conjugated using iEDDA click chemistry to barcode oligos as described before[46]. In addition, we included some commercially available Totalseq-A antibodies (Biolegend). Post-sorting and staining, cells were run through the standard 10x Chromium (v3) protocol up until cDNA amplification, with the following modification: For the cDNA PCR step, 0.2uM of ADT additive primer (5'CCTTGGCACCCGAGAATTCC) and 0.2uM of HTO additive primer (5'GTGACTGGAGTTCAGACGTGTGCTC) were added to the cDNA amplification master mix. Post cDNA amplification, a 0.6X SPRI cleanup was performed to separate the cDNA fraction (on beads) from the smaller ADT and HTO fractions (in supernatant). The cDNA fraction was converted into a 3' tag gene expression library according to the 10x Genomics Single Cell Genomics Protocol (v3). Supernatant from cleanup was kept for ADT and HTO preparation.

To the supernatant, another 1.4X SPRI was added to bring the total SPRI concentration to 2X. After washing the beads in 80% ethanol and eluting in water, a second round of 2X SPRI cleanup was performed to remove any residual primer carryover from the cDNA PCR. Post cleanup, eluate was taken into ADT PCR amplification (using TruSeq Small RNA RPIx primer (5'CAAGCAGAAGACGGCATACGAGxrefXXGTGACTGGAGTTCCTTGGCACCCGAG AATTCCA) and SI PCR primer (5'AATGATACGGCGACCACCGAGATCTACACTCTTTCCCTACACGACGCTC)), and into hashtag amplification (using TruSeq D7xx (5'CAAGCAGAAGACGGCATACGAGATxrefXXGTGACTGGAGTTCAGACGTGTGC) and SI PCR primers). Libraries were pooled and sequenced on a 100 cycle Novaseq S1 flowcell, with the configuration of 30 base pairs for R1, and 92 base pairs for R2. Additional protocol details can be found for CITE-seq and cell hashing at www.cite-seq.com.

Post sequencing, gene expression count matrices were generated using cell ranger version 5.0 using the refdata-gex-mm10-2020-A reference library provided by 10x Genomics, with the additional sequences of cre, eGFP, and tdTomato. Counts matrices for hashtags and antibodies were generated using kallisto bustools (kallisto v0.46.0, bustools v0.39.3). Downstream analysis was then performed in R using Seurat. Code for generating counts matrices can be found at https://github.com/nygctech/Kedmi-CITEseq.

Quality control and doublet removal: We initially selected all cells that were detected in our RNA-seq, cell hashing, and ADT libraries. We removed cells with < 700 detected genes, but also removed cells which had an aberrantly high number of genes (more than 5,000 genes) and a high percentage of mitochondria genes (more than 6%). Additionally, we removed the cells which were attached by the clumps of antibodies and had a too high number of ADT or HTO UMIs (more than 5,000 ADT UMI and 4,000 HTO UMI). We

used our previously described hashing-based doublet detection strategy[45], implemented in HTODemux, to identify doublets that represent two or more cells representing different samples. Only Singlet cells were used for the downstream analysis.

Multimodal analysis: We normalized RNA data using SCTransform[47] and applied the centered-log ratio (CLR) transformation to normalize ADT data within each cell. We used principal component analysis (PCA) to reduce dimensionality of both datasets. Then we took both top 20 RNA and protein PCA dimensions as the input of weighted nearest neighbors (WNN) method[48] to construct the multimodal weighted KNN graph. To cluster our multimodal dataset, we first used the weighted KNN graph to generate a shared nearest neighbor graph (SNN) and then apply the graph-based smart local moving (SLM) algorithm (https://doi.org/10.1140/epjb/e2013-40829-0) on this SNN graph to find clusters with 0.8 resolution. We performed differential expression on all pairs of clusters for both RNA and protein markers, and merged clusters that did not exhibit clear evidence of separation. All samples were clustered together and separated later for further analysis as indicated.

'Home-made' barcoded antibodies: SIRPa_CD172a (P84), GAGTAGCACATAAAA; SiglecH (551), CGTGATTGAAGGAAA; SiglecF (S17007L), CGAAGAGGCCTTAAA; PDL1 (10F), TAGGAATGCTCGAAA; PDCA1_CD137 (17B5), TTCGTACAGTTCAAA; PD1 (RMP1-14), TGCTTCGCATGGAAA; NK1.1 (PK136), AGCAAGCCTCATAAA; MERTK (2B10C42), AGCTGCCACTACAAA; Ly6D (49-H4), CTTGTATGTAGGAAA; IL7Ra_CD127 (A7R34), CGGAGTAGTAATAAA; IA/IE (M5/114.15.2), TGGCTGGCTAGAAAA; Flt3 (A2F10), TAGCCGATCACGAAA; F4/80 (BM8), GTCGCTTAGCACAAA; CX3CR1 (SA011F11), CTCTACTTGCCGAAA; CSF1R_CD115 (AFS98), TTGATCGACCGTAAA; CLEC9A_DNGR1_CD370 (7H11), TGAGCCTCACTTAAA; CLEC12A_CD371 (5D3/CLEC12A), GAACTTCTGGCGAAA; cKit (2B8), CCTCGGATACTAAAA; CD86 (GL-1), ATGTCTAGGTACAAA; CD80 (16-10A1), AGTCATAGCCGCAAA; CD8 (5H10),CCGATCGTATGCAAA; CD74 (In1/CD74), TATACGGACGTGAAA; CD71 (RI7217),TAGGCTGCTTAAAAA; CD69 (H1.2F3), ACGGCTAATCACAAA; CD54 (YN1/1.7.4), GGACATTACCACAAA; CD44 (IM7), CTCAGATCTACCAAA; CD40 (x 03/23), CAGTACGTATTCAAA; CD4 (RM4-5), TGACGTAACACTAAA; CD38 (90), GGCCGAGTCTAAAAA; CD370 (7H11), GATCGTGTTGGCAAA; CD317 (REA818), GTCTGTAGGCATAAA; CD29 (HMB1-1),TTCACTGGCTAAAAA;CD273 (TY25), GACGTGGCCTAAAAA; CD26 (H194-112), GCTTAGCTCGGAAAA; CD24 (M1/69), TAGTGCTAGGCGAAA; CD209a (MMD3), CAATAGCAGCTCAAA; CD205 (NLDC-145), TCTGGAGGACAAAAA; CD16/32 (93), CAGTTGCTCTGAAAA; CD154 (MR1), CTCGAGTGAATCAAA; CD14 (Sa14-2), AAGGTGTCAGGCAAA; CD127 (A7R34), CGTACAAGCCACAAA; CD11c (N418), CGTAAGAACCGTAAA; CD11b (M1/70), TCAATTGCGTGCAAA; CD103 (2E7), CCGCGTTACACAAAA; CCR9_CD199 (L053E8), ACCGATCTCAGCAAA; CD62L (MEL-14), AATCGCTCCGGAAAA; Ly6B2 (7/4), TTGTATCTCCACAAA; ESCAM (AF2827), ATAGGTCATGCGAAA; Notch1(HMN1-12), GCTCAGATTAGTAAA; TNF,TCTCTCAAGTCCAAA;Notch2 (HMN2-35), CATACGCGAAGGAAA. All antibodies were obtained from BioLegend, except for Ly6D that was obtained from BD Pharmingen, flt3 that was obtained from eBioscience and ESAM and TNF that were purchased from R&D systems.

CITEseq antibodies were used at concentration of 1ug/100ul. Antibodies that show differential staining pattern were considered as validated antibodies.

Single cell RNAseq of Aire⁺ cells

Four-week-old Adig mouse lymph nodes (cervical, brachial, axillary, inguinal, and mesenteric) (n=3) were pooled in digestion medium consisting of RPMI 1640 with 2% fetal bovine serum (FBS) (Sigma-Aldrich), deoxyribonuclease (DNase) (100 μg/ml; Roche) and Liberase (50 μg/ml; Roche), minced and agitated at 37°C for 30 min, and passed through a 70-μm filter. Cells were resuspended for magnetic column enrichment (Miltenyi LD column depletion with streptavidin microbeads and biotinylated antibodies against B220, Ter119, TCRbeta, CD3e). Cells were then either processed directly for 10x single-cell analysis as reference sample or sorted by flow cytometry for all live GFP+ cells. Cells were sorted into PBS with 0.04% bovine serum albumin (BSA). Cell viability and counts were evaluated with Vi-CELL XR (Beckman Coulter), and samples with viability >85% were used for sequencing.

For analysis, sequencing files were aligned to the mm10 mouse reference genome with the 10x Genomics Cell Ranger (v3.1.0) count method using the default parameters. Raw count files were then processed in Python (v3.9.7), removing doublets from each sample using Scrublet[49] with a doublet score threshold of 0.3. Samples were merged and filtered, removing genes with no counts, and retaining cells with 600 to 5,000 genes and 1,000 to 30,000 counts, leaving a total of 35,797 cells and 22,979 genes in the dataset. The raw counts were used to train a model of gene expression using scvi-tools (v0.14.6) with each sample as a batch key. This model was used to generate normalized expression values for all genes scaled to a library size of 100,000 and create a tSNE representation of the data using Scanpy[50] (v1.8.2) with the default parameters. Leiden clustering with a resolution of 0.8 gave 29 clusters which were assigned cell types after removing three low quality clusters. For targeted analysis of JC, the data was subset on the three JC clusters and a UMAP was created using Scanpy with a minimum distance of 0.5 and spread of 1. Differential gene expression of JC clusters was performed using scvi-tools[51], filtering on genes with a bayes factor greater than 3, mean log fold change greater than 0, and proportion of cells with non-zero expression greater than 0.1. The z-score of the average expression of the top 10 DE genes from each cluster was used for visualization. For low-dimensional embeddings of feature plots, scVI normalized expression was used, clipping the top and bottom 1% of expression values in the full dataset to the maximum and minimum of the color scale to prevent outliers from skewing the visualization. To display expression of key features in dotplots, log-normalized and scaled counts for each gene were averaged and standardized across cell types to have a value ranging from 0 to 1.

RNAscope

Fresh-frozen spleen and lymph nodes were sectioned at 8um and then fixed overnight at 4°C in 10% neutral buffered formalin (Thermo Fisher Scientific, Waltham, MA) before proceeding with an RNAscope RED 2.5 HD Chromogenic Assay kit (Advanced Cell Diagnostics, Newark, CA) for detection of Aire mRNA. DapB probe was used as negative

control and Polr2a probe was used as positive control. Semi-quantitative scores were determined in a blinded fashion based on the number of Aire^{+} cells per section.

Integrin β₈ (ADWA-11) blocking Ab

We injected IP 200ug of ADWA-11 into mice colonized with Hh for 7 days. On the same day we adoptively transferred 100K CFSE-labeled naive Hh7-2 cells and tested their proliferation and differentiation in the C1 MLN, 3 days after the transfer.

Generation of bone marrow (BM) chimeric reconstituted mice

To generate chimeric mice, 4–5 week old CD45.1 mice were irradiated twice with 500 rads/mouse at an interval of 2–5 h (X-RAD 320 X-Ray Irradiator). A day after, bone marrow (BM) mononuclear cells were isolated from donor mice, as indicated in each experiment, by flushing the femur bones. Red blood cells were lysed with ACK Lysing Buffer, and lymphocytes were depleted for Thy1.2 using magnetic microbeads (Miltenyi). BM cells were resuspended in PBS and a total $3–4 \times 10^6$ BM cells were injected intravenously into the irradiated mice. In case of mixed BMC reconstitution, a ratio of 1:1 was used. Mice were kept for a week on broad spectrum antibiotics (1 mg/mL sulfamethoxazole and 0.2 mg/ mL trimethoprim), followed by microbiome reconstitution by fecal gavage. Mice were reconstituted for 1–2 months before Hh colonization. After 7 weeks, peripheral blood samples were collected and analyzed by FACS 7 to check for reconstitution.

Intravital multiphoton microscopy

Naive Hh7-2 T cells were isolated from *Nur77-eGFP* Hh7-2tg mice, labeled with Cell tracker dye (eBioscience Cell Proliferation Dye eFluor 450), and transferred into *mKate2-ON^zbtb46^;RORγt-eGFP* mice that had been colonized with Hh for 6 days. Fifteen hours following adoptive transfer of Hh T cells, mice were euthanized and C1 MLN were immediately isolated and mounted in cold RPMI with 10% FCS for intravital multiphoton microscopy. Image stacks were acquired with an Olympus multiphoton FVMPE-RS system equipped with both InSight X3 and Mai Tai Deepsee (Spectra-Physics) tunable Ti:Sapphire lasers, using Fluoview software. To acquire serial optical sections, a laser beam (780 nm for eFluor™ 450 and 940 nm for simultaneous excitation of eGFP and mKate2) was focused through a water immersion lens (N.A. 1.05; Olympus) and scanned with a field of view of 0.5 mm², at 600 Hz. Z-stacks were acquired in 2 mm steps to image a total depth of 150–200 mm of tissue.

Image analysis

Raw image stacks were imported into Fiji (NIH) for T cell colocalization analysis. Provided images are presented as a maximal projection of 3–6 mm optical sections. For visualizing individual labelled cells expressing both the mKate2 and eGFP, the brightness and contrast were adjusted accordingly to single positive green (eGFP) and red (mKate2) cells. Adoptively transferred Hh7-2tg T cells were identified via positive labeling with cell proliferation dye eFluor 450. Primed Hh7-2tg T cells were identified via expression of the *Nur77-eGFP* reporter. Cell identity was scored by a combination of both fluorescent reporter expression as well as cell morphology. Specifically, cells expressing mKate2 with a dendritic

cell shape were scored as cDC, while cells expressing both *RORγt-eGFP* and mKate2 (or *eGFP* alone) with an amoeboid (non-spherical) cell shape were scored as ILC3. T cell interactions with cDC or ILC3 was strictly measured as direct (<1 micron) colocalization of cells with respective fluorescent and cell morphology combinations.

Statistical analysis

For animal studies, mutant and control groups did not always have similar standard deviations and therefore an unpaired two-sided Welch's t-test was used. Error bars represent ± s.d. Animal sample size estimates were determined using power analysis (power = 90% and $\alpha = 0.05$) based on the mean and s.d. from our previous studies and/or pilot studies using 4–5 mice. No samples were excluded from analysis. For analysis of ILC3 counts in MLN and LP of chimeric mice, a paired two-sided t-test was used.

Data availability

Data generated for this project are available at the Gene Expression Omnibus with the accession code GSE200148. Published data GSE176282 was used for analysis. Refdata-gex-mm10-2020-A reference library provided by 10x Genomics was used to generate gene expression count matrices.

Code availability

All code used for analysis in this manuscript is available at https://github.com/nygctech/Kedmi-CITEseq.
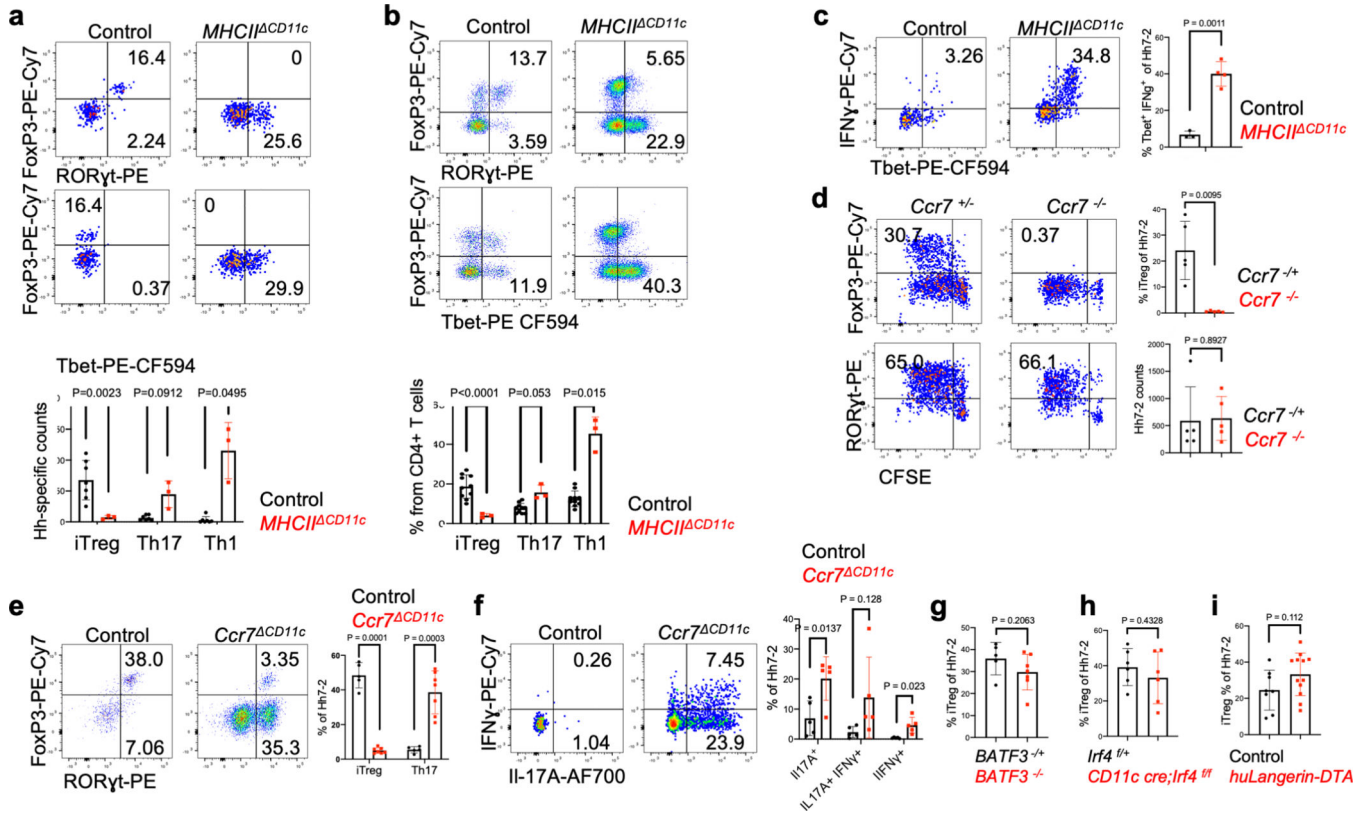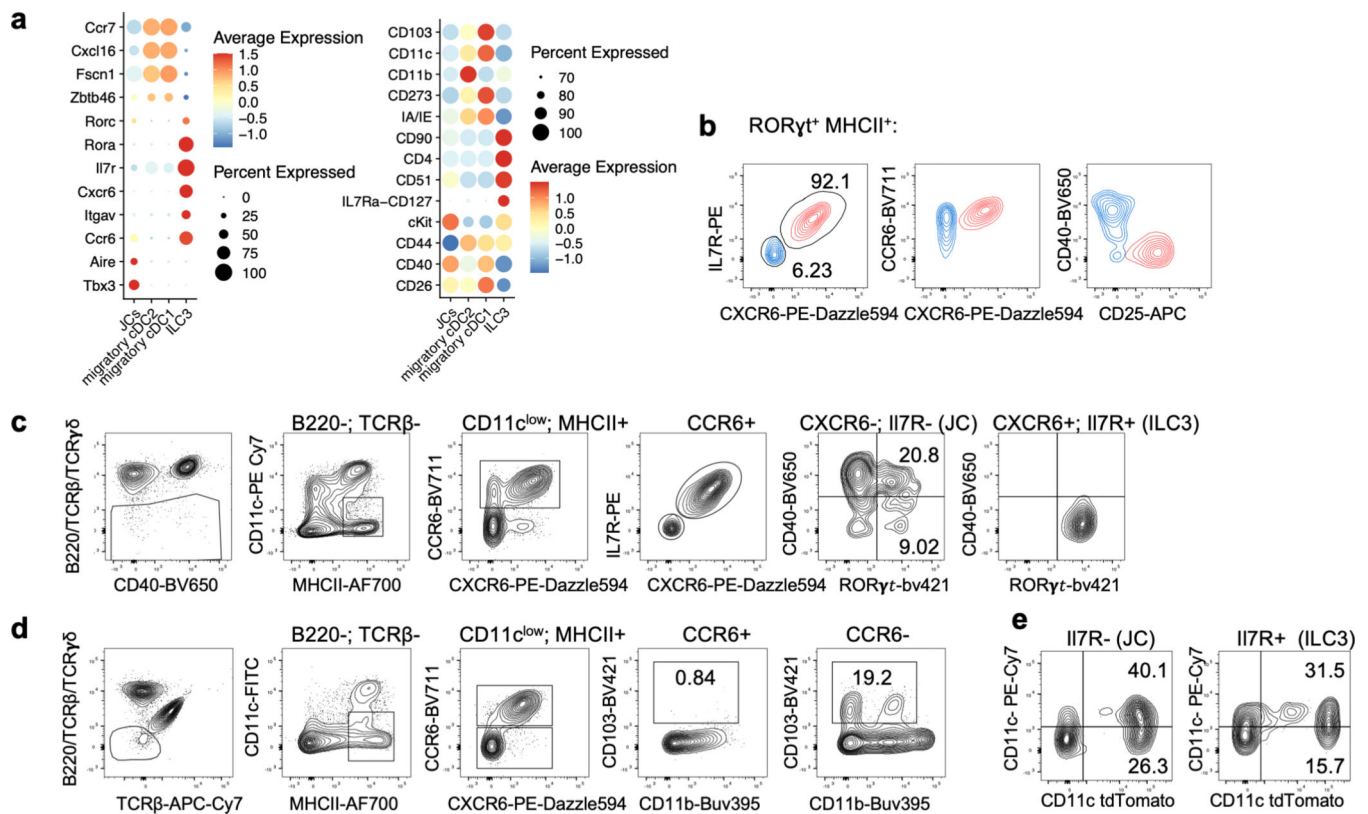
Extended Data

Extended Data Fig. 1. Cells targeted by CD11c-Cre and consequences for Hh-specific T cell differentiation.

a, Phenotype of Hh7–2 TCR transgenic T cells in the colon lamina propria at 10 days after transfer into Hh-colonized *MHCII* ^{CD11c} (n=3) and control mice (n=7), as indicated. **b,** Phenotype of host CD4$^+$ T cells from mice in (a); *MHCII* ^{CD11c} (n=3) and control mice (n=10), as indicated. **c,** Cytokine profile of Hh7–2 T cells shown in (a); *MHCII* ^{CD11c} (n=4) and control mice (n=3). **d,** Proliferation and differentiation of Hh-specific iTreg and Th17 cells in the MLN of *Ccr7*$^{-/-}$ (n=5) and littermate control mice (n=5). CFSE-labeled Hh7–2 T cells were analyzed at 3 days following their adoptive transfer into Hh-colonized mice. Data summarize two independent experiments. **e-f,** Transcription factor (e) and intracellular cytokine (f) profiles of Hh7–2 T cells in the large intestine of *Ccr7* ^{CD11c} (n=7 or 5, for transcription factors and cytokines, respectively) and littermate control (n=5) mice, at 10 days after adoptive transfer. **g-i**, Proportion in MLN of Hh7–2 with the iTreg phenotype at 3 days after transfer into *BATF3*$^{-/-}$ (g) (n=7), *IRF4* ^{CD11c} (h) (n=6), and *huLangerin (CD207)-DTA* (i) (n=12) mice (red) and indicated littermate controls (black). Data summarize at least two independent experiments. Representative flow panels and aggregate data are shown for each analysis. All statistics were calculated by unpaired two-sided Welch's t-test. Error bars denote mean ± s.d. *p*-values are indicated in the figure.
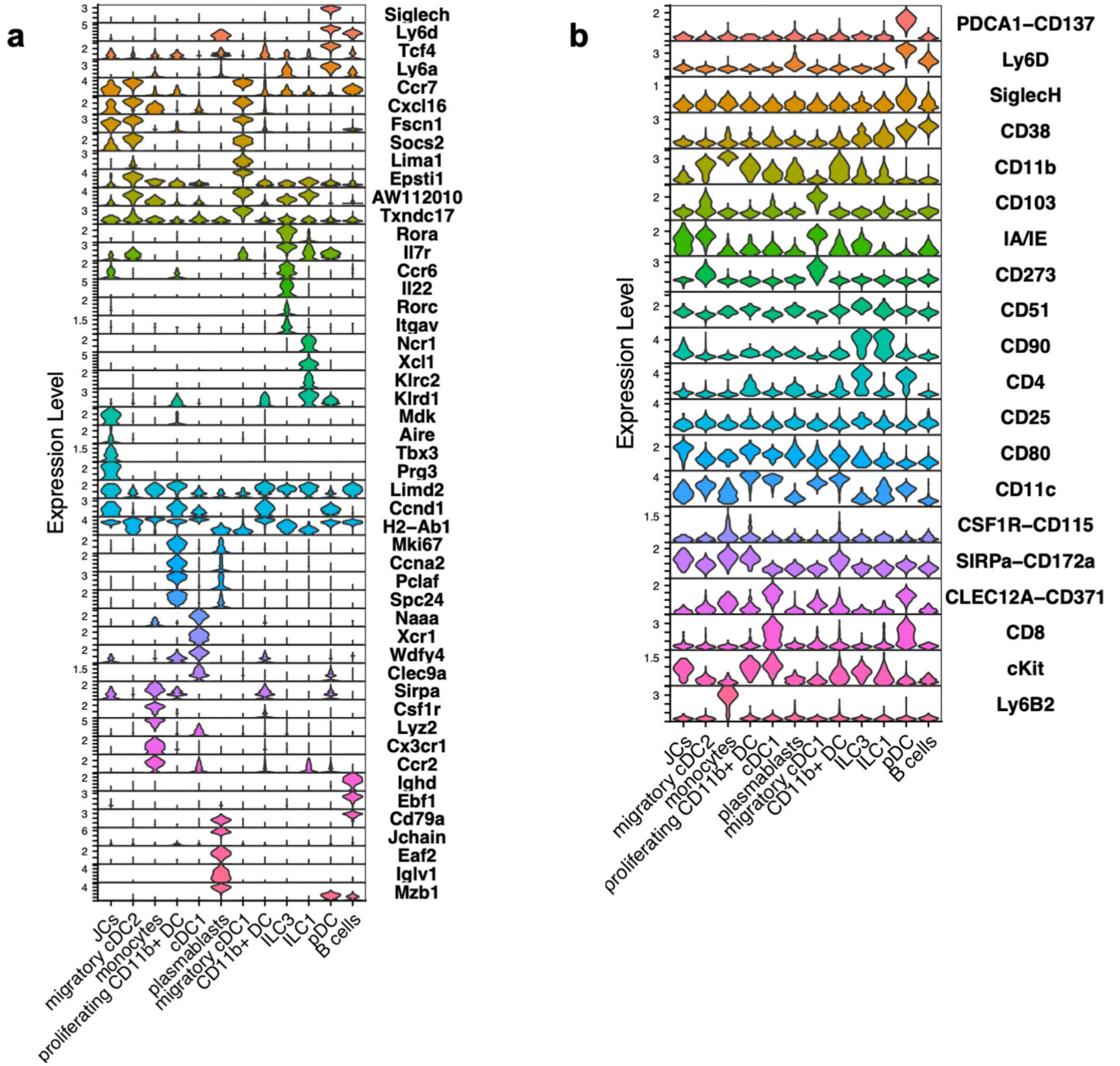
Extended Data Fig. 2. Identification of CITE-seq-assigned clusters of sorted *tdTomato-ON* CD11c fate-mapped cells.

a, Stacked violin plots for selected (curated) and top DEG (data-driven) of tdTomato+ cells sorted from MLN of Hh-colonized mice. **b,** Stacked violin plots for selected (curated) cell surface markers for each cluster.

Extended Data Fig. 3. Phenotypic discrimination of ILC3 and JC.
a, Dot plots for selected (curated) DEG and cell surface markers for the indicated clusters, obtained from CITE-seq analysis of *tdTomato-ON* ^{CD11c} fate-mapped cells. **b,** Flow cytometry profiling of CXCR6, CD127(IL-7R), CCR6 CD25 and CD40 on ILC3 (red) and JC (blue), pre-gated on TCRβ⁻, TCRγδ⁻, B220⁻, RORγt⁺, MHCII⁺. **c,** gating strategy for JC using cell surface staining as indicated. **d,** Flow cytometry profiling of JC and DC markers, showing that migratory cDC are excluded from CD11c^low CCR6⁺ gating. **e,** TdTomato levels in ILC3 (TCRβ⁻, TCRγδ⁻, B220⁻, MHCII⁺ CCR6⁺, Il7R⁺) and JC (TCRβ⁻, TCRγδ⁻, B220⁻, MHCII⁺ CCR6⁺, Il7R⁻) from the MLN of Hh-colonized *tdTomato-ON^CD11c* fate-map mice.
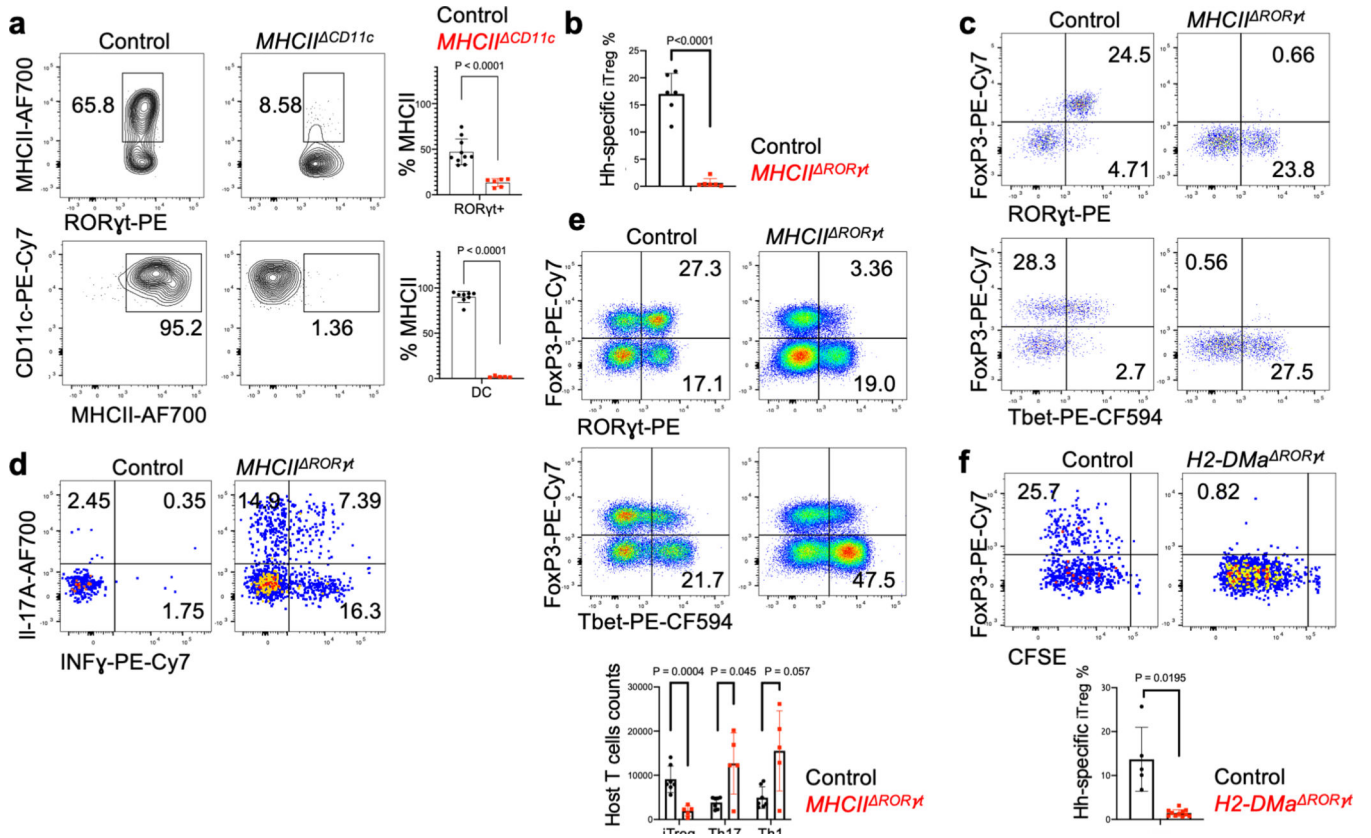
Extended Data Fig. 4. Antigen presentation by RORγt⁺ cells is required for microbiota-induced iTreg cell differentiation.

a, MHCII expression in RORγt⁺ cells (top) and DC (bottom) from the MLN of Hh-colonized *MHCII* ^{ΔCD11c} mice (n=6 and 5) and littermate controls (n =10 and 8). RORγt⁺ cells were gated as TCRβ⁻, TCRγδ⁻, B220⁻, RORγt⁺; DC were gated as TCRβ⁻, TCRγδ⁻, B220⁻, CD90⁻, CD11cʰⁱᵍʰ. **b,** Bar graph showing frequency of iTreg among Hh7–2 T cells, measured as in Figure 2e. **c-d,** Representative dot plots showing Hh7–2 T cell differentiation (c) and cytokine (d) profiles in colon lamina propria at 22 days after adoptive transfer into Hh-colonized *MHCII* ^{ΔRORγt} and littermate controls. **e,** Representative and aggregate data of transcription factor profiles of host CD4⁺ T cells in colon lamina propria of mice shown in (c) and (d). **f,** Hh7–2 cell proliferation and differentiation in the MLN of *H2-DMa* ^{ΔRORγt} (*RORγt-Cre; H2-Dma* $^{f/f}$) (n=11) and littermate controls (*RORγt-Cre; H2-DMa* $^{+/f}$) (n=5) at 3 days after transfer of CFSE labeled naïve Hh7–2, cell proliferation and FoxP3 were assessed in cells isolated from C1 MLN. Representative flow cytometry (left) and aggregate data from multiple animals (right). Data summarize two independent experiments. All statistics were calculated by unpaired two-sided Welch's t-test. Error bars denote mean ± s.d. *p*-values are indicated in the figure.
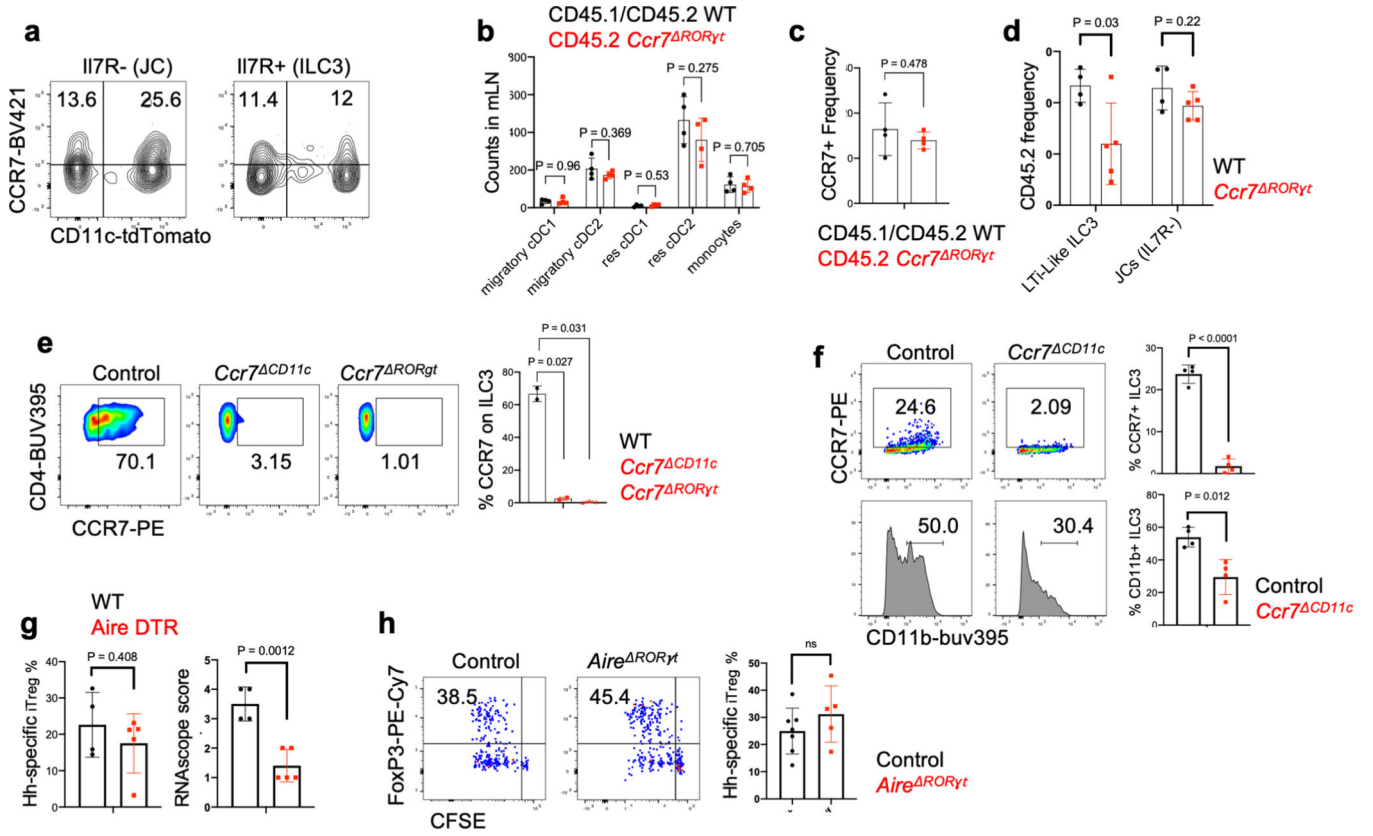
Extended Data Fig. 5. Differential requirements for CCR7 in iTreg and effector Th17 cell differentiation and analysis of Aire$^+$ JC function in differentiation of Hh-specific iTreg cells.
a, Cell surface expression of CCR7 on *CD11c-Cre* fate-mapped ILC3 (TCRβ$^-$, TCRγδ$^-$, B220$^-$, MHCII$^+$, CCR6$^+$, IL-7R$^+$) and JC (TCRβ$^-$, TCRγδ$^-$, B220$^-$, MHCII+, CCR6+, IL-7R$^-$) in the MLN. **b-c,** Analysis of DC counts in MLN (b) and large intestine (c) of WT and *Ccr7* ^{RORγt} mixed bone marrow chimeric mice described in Figure 3c. Counts in the MLN of DC subsets derived from bone marrow (b); frequencies of CCR7$^+$ among total colonic DCs (c) (n=4). Statistics were calculated using paired two-sided t-test. **d,** Analysis of CD45.2 frequencies within donor cells is presented for ILC3 (TCRβ$^-$, TCRγδ$^-$, B220$^-$, MHCII$^+$, RORγt $^+$, IL-7R$^+$) and JC (TCRβ$^-$, TCRγδ$^-$, B220$^-$, MHCII$^+$, RORγt $^+$, IL-7R$^-$) in the MLN of WT and *Ccr7* ^{RORγt} mixed bone marrow chimeric mice described in Figure 3c. **e,** Cell surface expression of CCR7 in colonic ILC3 (TCRβ$^-$, TCRγδ$^-$, B220$^-$, CD90$^+$, RORγt$^+$, CD25$^+$, CD4$^+$) from *Ccr7* ^{RORγt} (n=3), *Ccr7* ^{CD11c} (n=2) and control Hh-colonized mice (n=2). **f,** Cell surface expression of CCR7 and CD11b in ILC3-gated MLN cells (TCRβ$^-$, TCRγδ$^-$, B220$^-$, IL-7R$^+$, CCR6$^+$, CD25$^+$) from *Ccr7* ^{CD11c} (n=4) and control Hh-colonized mice (n=4). **. g,** Lethally irradiated mice were reconstituted with BM cells from CD45.2 *Aire-DTR* or CD45.2 WT mice. One month after reconstitution, mice were colonized with Hh, and one week later were treated with Diphtheria toxin (DT, Sigma-Aldrich) for 3 sequential days (at a dose of 25 ng/g mice). CD45.1/CD45.2 CFSE-labeled Hh7–2 T cells (1×10^5) were transferred intravenously into the mice on the first day of DT treatment. Bar graph of proportion of proliferating Foxp3$^+$ Hh7–2 T cells in the MLN of mice reconstituted with Aire-DTR BM (n=5) or with WT BM (n=4) (left); *Aire* mRNA in

the spleen of the treated mice was blindly scored using RNAscope analysis. The experiment was performed once. **h,** Proliferation and differentiation of CFSE-labeled Hh7–2 T cells in the MLN of *RORγt-Cre;Aire^{f/f}* (n=5) and control *Aire^{+/f}* littermates (n=7) at 3 days after adoptive transfer. Data summarize three independent experiments. All statistics, except for b and c, were calculated by unpaired two-sided Welch's t-test. Error bars denote mean ± s.d. *p*-values are indicated in the figure.
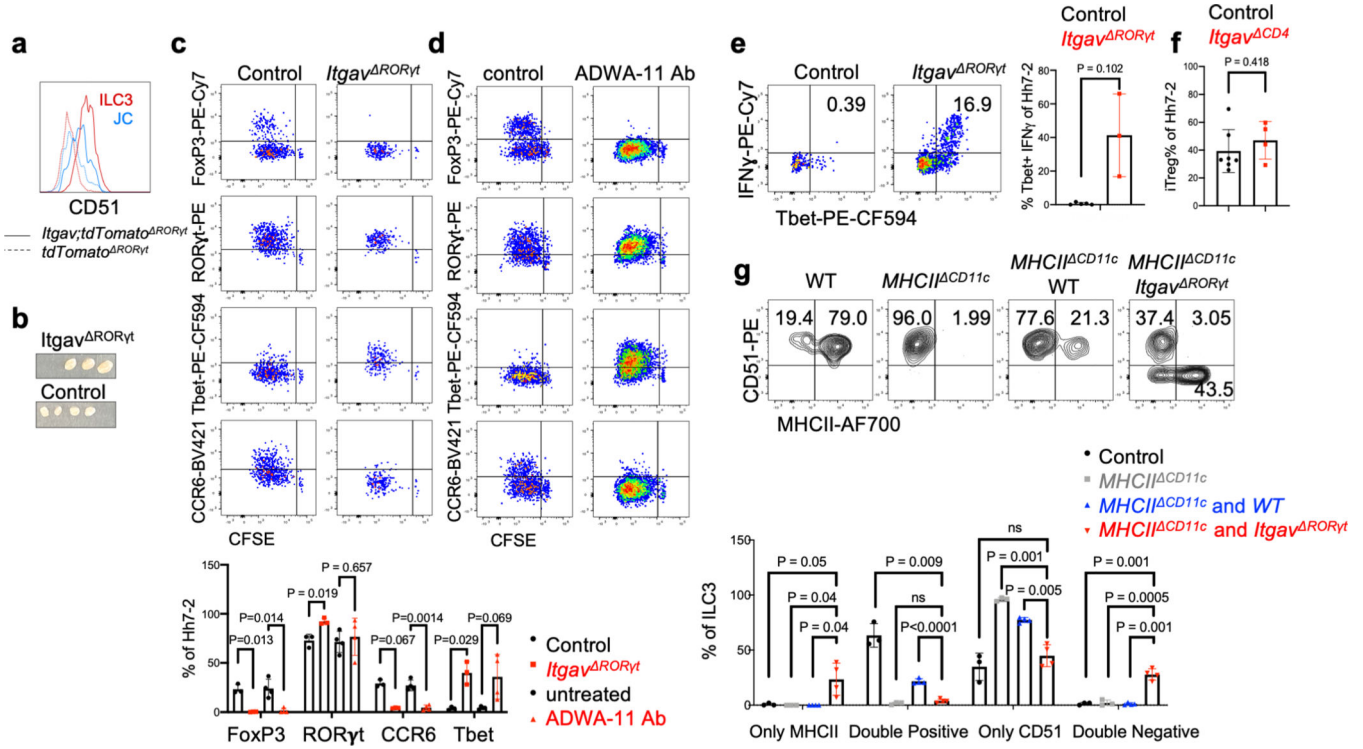
Extended Data Fig. 6. Effect of integrin α_vβ_8 blockade or α_v inactivation on microbiota-dependent T cell differentiation.

a, Expression of integrin α_v (CD51) in fate-mapped RORγt^+ cell subsets from MLN of wild type and *Itgav^{ΔRORγt}* mice. **b,** C1 MLN from *Itgav^{ΔCD11c}* (n=3) and littermate controls (n=4), 10 days after Hh colonization. **c-d,** Flow cytometry profiling of transcription factors and CCR6 in proliferating CFSE-labeled Hh7–2 in the MLN at 3 days after adoptive transfer into *Itgav^{ΔRORγt}* (n=3) and littermate control mice (n=3) (b) or into mice treated with ADWA11(n=4) (as in Fig. 4a) or untreated control littermates (n=4) (c). Summary data of results in (b) and (c) are shown below. **e,** Intracellular IFNγ and T-bet expression in PMA/Ionomycin-stimulated Hh7–2 T cells isolated from colon lamina propria of *Itgav^{ΔRORγt}*(n=3) and control littermates (n=5), 10 days after adoptive transfer. **f,** Frequency of iTreg cells among proliferating Hh7–2 in the MLN at 3 days after adoptive transfer into *Itgav^{ΔCD4}* (n=4) and control littermates (n=7). Data summarize two independent experiments. **g,** Integrin α_v and MHCII cell surface expression in ILC3 (gated as TCRβ^−, TCRγδ^−, B220^−, RORγt^+, CD90^+, CD25^+ CD45.2^+) isolated from MLN of bone marrow chimeric mice, reconstituted with different combinations of donor cells as indicated and colonized with Hh for 10 days. Data summarized below for control (n=3), *MHCII^{ΔCD11c}* (n=3), *MHCII^{ΔCD11c}* and WT (n=4), and *MHCII^{ΔCD11c}* and *Itgav^{ΔRORγt}*

(n=4) reconstituted mice. All Statistics were calculated by unpaired two-sided Welch's t-test. Error bars denote mean ± s.d. *p*-values are indicated in the figure.
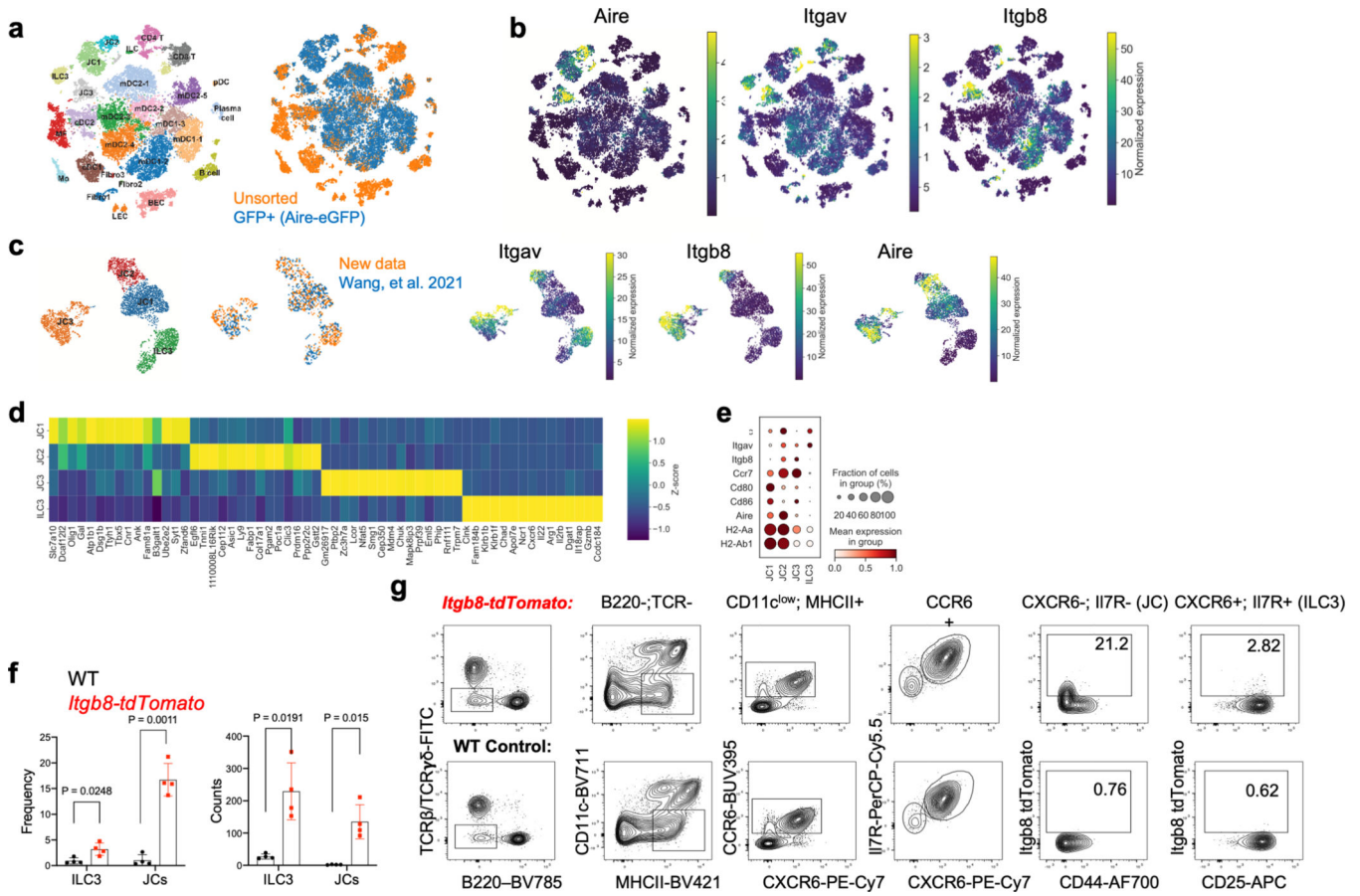
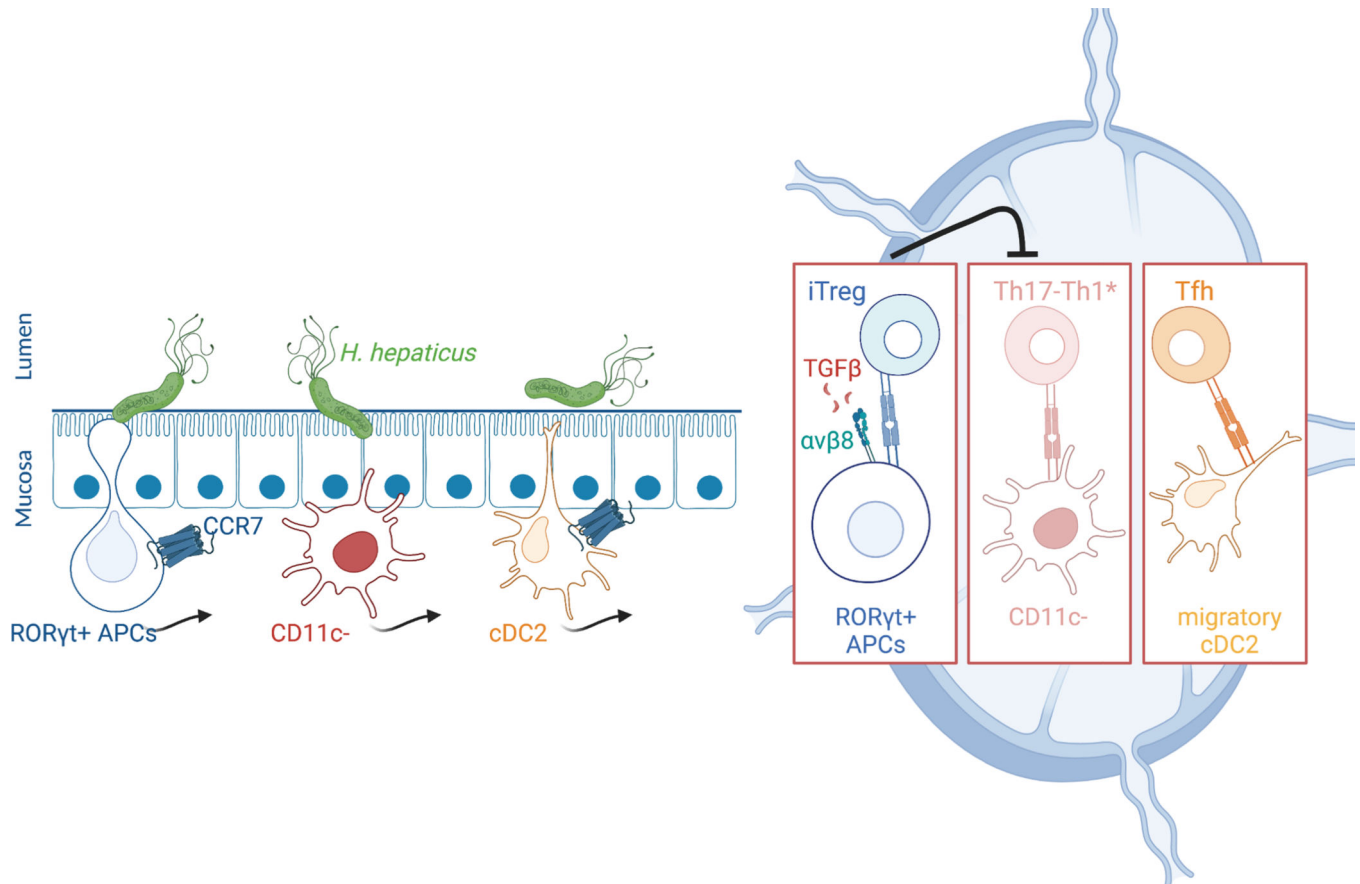**Extended Data Fig. 7.** *Itgav and Itgb8 expression in ILC3 and JC.*

a, tSNE plot with Leiden clustering of scRNAseq of pooled GFP+ sorted and unsorted cells, as indicated, from pooled lymph nodes of Adig mice[32]. **b,** tSNE feature plots showing *Aire, Itgav, and Itgb8* levels in the cell clusters. **c,** UMAP plot of Aire+ JC and ILC3 populations from pooled datasets as indicated with associated feature plots. **d,** top differentially expressed genes per pseudobulk cluster in (c), shown by heatmap. **e,** dot plot of selected genes in JC and ILC3 clusters. **f-g,** aggregate results (f) and representative flow cytometry (g) of tdTomato+ JC and ILC3, gated as indicated, in C1 MLN of *Itgb8-IRES-tdTomato* mice[33] (n=4) and littermate controls (n=4). Aggregate data (right) show percent tdTomato+ cells among total ILC3 and JC and number of reporter-positive cells in the C1 MLN of each mouse. We performed two independent experiments and data shown are from one representative experiment. All statistics were calculated by unpaired two-sided Welch's t-test. Error bars denote mean ± s.d. *p*-values are indicated in the figure.
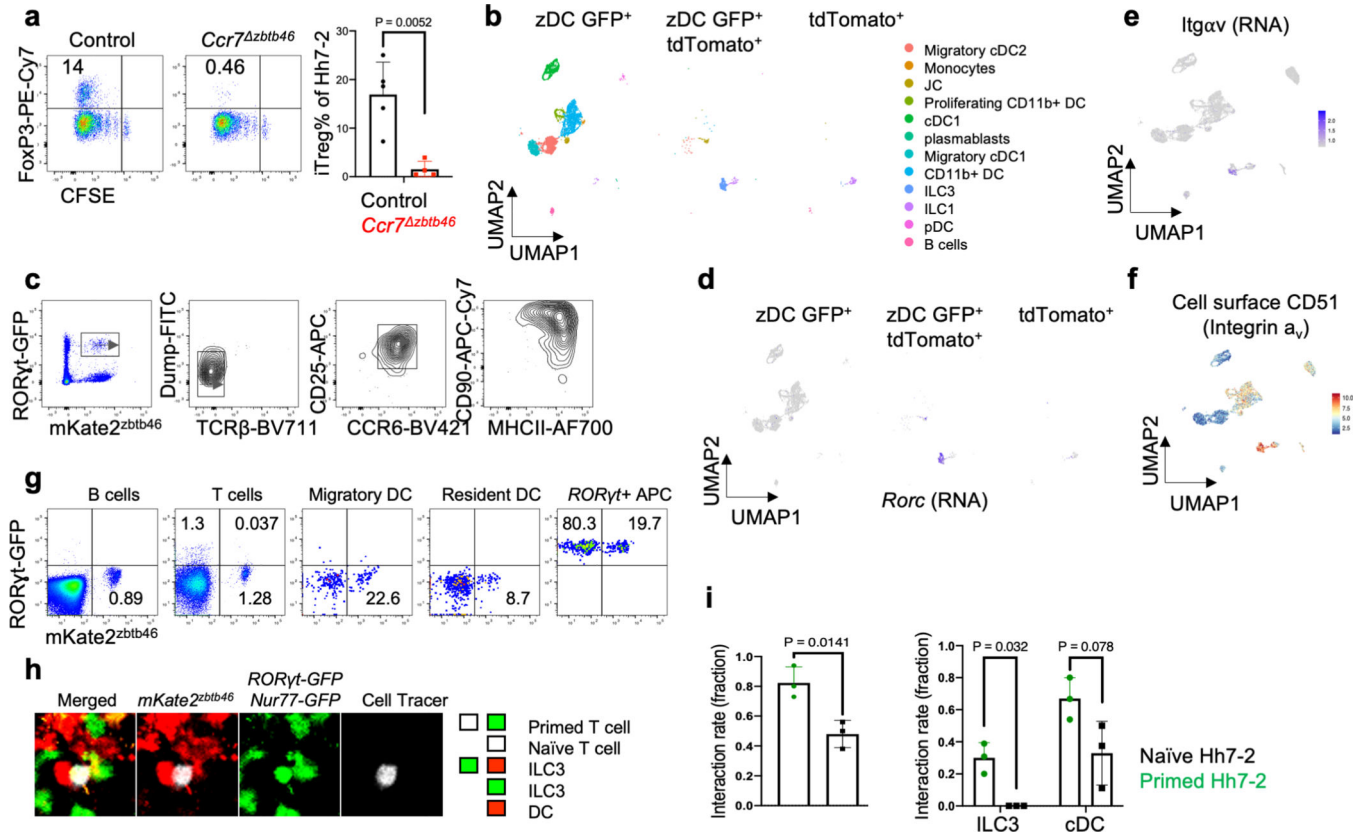
Extended Data Fig. 8. Analysis of RORγt-expressing cells in the MLN and intravital tracking of RORγt-expressing cells and DC interactions with Hh-specific T cells during priming in the MLN.

a, Hh7–2 proliferation and differentiation in MLN of *Ccr7* ^{zbtb46} (n= 4) and control littermates (n=5), at 3 days after transfer of the naïve cells. Data in the right panel summarize three independent experiments. **b,** UMAP visualization of CITE-seq datasets obtained from 3 distinct sorted populations (GFP+, GFP+ tdTomato+ and tdTomato+) isolated from C1 MLN of *Zbtb46-eGFP ; tdTomato-ON* ^{RORγt} mice (n=2), analyzed by the WNN method. **c,** Flow cytometry analysis of fate-mapped C1 MLN cells from *RORγt-eGFP;mKate2-ON* ^{zbtb46} mice, gated for the indicated cell subsets. **d-e,** Feature plot showing *Rorc* (d) and integrin α_v (e) levels in the cell clusters identified in the CITE-seq analysis shown in (b); Positive cells are layered in front. **g,** Flow cytometry analysis of fate-mapped C1 MLN cells from *RORγt-eGFP;mKate2-ON* ^{zbtb46} mice, gated for the indicated cell subsets (ILC3 were gated as TCRβ−, TCRγδ−, B220−, MHCII+, RORγt-eGFP+, CCR6+, CD25+ and JC as TCRβ−, TCRγδ−, B220−, MHCII+, RORγt-eGFP+, CD25−). Note that there is incomplete excision of the transcriptional stop signal by *zbtb46-Cre*. **h,** Representative image of cell-cell interactions of recently primed Hh-specific T cells with DC and RORγt-expressing cells. *Nur77-eGFP* tracer-labeled Hh7–2 T cells were transferred into of *RORγt-eGFP;mKate2-ON*^{zbtb46} Hh-colonized mice. Cell colocalization of primed Hh7–2 (tracer dye+, GFP+) or naïve Hh7–2 (tracer dye+, GFP−) T cells with cDC (mKate2+ with dendritic morphology), RORγt-expressing cells (eGFP+, mKate2+ or eGFP+ alone with amoeboid morphology), or both were visualized using intravital multiphoton microscopy of the C1 MLN at 15 h after transfer. Note that Cell Tracer fluorescent labeling provides clear

spatial discrimination of *RORγt-eGFP* and *Nur77-eGFP* expressing cells. **i,** Quantification and graphical representation of the total (left) and individual rates of interaction of RORγt-expressing cells or cDC populations (right) with primed or naïve Hh7–2 T cells. Data summarize cell-cell interactions from six 0.25mm^3 three-dimensional regions of C1 MLN, (n=72 total Hh7–2 T cells), (n=49 primed and 23 naïve Hh7–2 T cells). All statistics were calculated by unpaired two-sided Welch's t-test. Error bars denote mean ± s.d. *p*-values are indicated in the figure.

Extended Data Fig. 9. Gain-of-function expression of MHCII in RORγt$^+$ cells rescues bone marrow-derived iTreg cell differentiation.

a, Aggregate data showing MHCII frequency on donor-derived DC and RORγt$^+$ cells in MLN and colon lamina propria from chimeric mice reconstituted with combinations of donor BM cells as indicated, with representative flow cytometry panel in Fig. 5b. MLN: WT (n=5), *MHCII^{CD11c}* (n=5), *MHCII^{CD11c}* and WT (n=8), *MHCII^{CD11c}* and *MHCII-ON^{RORγt}* (n=7). Colon: WT (n=4), *MHCII^{CD11c}* (n=6), *MHCII^{CD11c}* and WT (n=8), *MHCII^{CD11c}* and *MHCII-ON^{RORγt}* (n=6). **b,** Donor bone marrow-derived CD4$^+$ T cell differentiation in colon lamina propria from chimeric mice reconstituted with combinations of BM cells as indicated. Representative flow panels (left) and aggregate data (right). WT (n=10), *MHCII^{CD11c}* (n=11), *MHCII^{CD11c}* and WT (n=8), *MHCII^{CD11c}* and *MHCII-ON^{RORγt}* (n=9). Colon: WT (n=4), *MHCII^{CD11c}* (n=6), *MHCII^{CD11c}* and WT (n=8), *MHCII^{CD11c}* and *MHCII-ON^{RORγt}* (n=7). **c,** Representative flow cytometry (left) and aggregate data (right) of Hh7–2 T cell differentiation in colon lamina propria of Hh-colonized bone marrow chimeric mice reconstituted with cells of indicated genotypes, 12 days after transfer of naive TCR transgenic T cells. WT (n=8), *MHCII^{CD11c}* (n=7), *MHCII-ON^{CD11c}* (n=5), and *MHCII-ON^{RORγt}* (n=4). Data summarize two or three independent

experiments. All statistics were calculated by unpaired two-sided Welch's t-test. Error bars denote mean ± s.d. *p*-values are indicated in the figure.

Extended Data Fig. 10. Schematic of the requirement of distinct APC subsets for T cell differentiation.
CCR7 and integrin $\alpha_v\beta_8$ are required in RORγt$^+$ APCs for iTreg cell differentiation. Note that other APCs, with differential requirements for CCR7 expression, are involved in the priming and differentiation of pathogenic Th17 and Tfh cells.

Supplementary Material

Refer to Web version on PubMed Central for supplementary material.

Acknowledgements

References

1. Hooper LV, Littman DR & Macpherson AJ Interactions between the microbiota and the immune system. Science 336, 1268–1273, doi:10.1126/science.1223490 (2012). [PubMed: 22674334]

2. Ansaldo E, Farley TK & Belkaid Y Control of Immunity by the Microbiota. Annu Rev Immunol 39, 449–479, doi:10.1146/annurev-immunol-093019-112348 (2021). [PubMed: 33902310]

3. Xu M et al. c-MAF-dependent regulatory T cells mediate immunological tolerance to a gut pathobiont. Nature 554, 373–377, doi:10.1038/nature25500 (2018). [PubMed: 29414937]

4. Chai JN et al. Helicobacter species are potent drivers of colonic T cell responses in homeostasis and inflammation. Science immunology 2, doi:10.1126/sciimmunol.aal5068 (2017).

5. Wang J, Lareau CA, Bautista JL, Gupta AR, Sandor K, Germino J, Yin Y, Arvedson MP, Reeder GC, Cramer NT, Xie F, Ntranos V, Satpathy AT, Anderson MS, Gardner JM Single-cell multiomics defines tolerogenic extrathymic Aire-expressing populations with unique homology to thymic epithelium. Sci. Immunol. 6 (2021).

6. Russler-Germain EV et al. Gut Helicobacter presentation by multiple dendritic cell subsets enables context-specific regulatory T cell generation. eLife 10, doi:10.7554/eLife.54792 (2021).

7. Darrasse-Jèze G et al. Feedback control of regulatory T cell homeostasis by dendritic cells in vivo. The Journal of experimental medicine 206, 1853–1862, doi:10.1084/jem.20090746 (2009). [PubMed: 19667061]

8. Durai V & Murphy KM Functions of Murine Dendritic Cells. Immunity 45, 719–736, doi:10.1016/j.immuni.2016.10.010 (2016). [PubMed: 27760337]

9. Esterházy D et al. Classical dendritic cells are required for dietary antigen-mediated induction of peripheral T(reg) cells and tolerance. Nature immunology 17, 545–555, doi:10.1038/ni.3408 (2016). [PubMed: 27019226]

10. Nussenzweig MC, Steinman RM, Gutchinov B & Cohn ZA Dendritic cells are accessory cells for the development of anti-trinitrophenyl cytotoxic T lymphocytes. The Journal of experimental medicine 152, 1070–1084, doi:10.1084/jem.152.4.1070 (1980). [PubMed: 6968335]

11. Nutsch K et al. Rapid and Efficient Generation of Regulatory T Cells to Commensal Antigens in the Periphery. Cell Rep 17, 206–220, doi:10.1016/j.celrep.2016.08.092 (2016). [PubMed: 27681432]

12. Esterhazy D et al. Compartmentalized gut lymph node drainage dictates adaptive immune responses. Nature 569, 126–130, doi:10.1038/s41586-019-1125-3 (2019). [PubMed: 30988509]

13. Worbs T et al. Oral tolerance originates in the intestinal immune system and relies on antigen carriage by dendritic cells. The Journal of experimental medicine 203, 519–527, doi:10.1084/jem.20052016 (2006). [PubMed: 16533884]

14. Koscso B et al. Gut-resident CX3CR1(hi) macrophages induce tertiary lymphoid structures and IgA response in situ. Science immunology 5, doi:10.1126/sciimmunol.aax0062 (2020).

15. Mildner A & Jung S Development and function of dendritic cell subsets. Immunity 40, 642–656, doi:10.1016/j.immuni.2014.04.016 (2014). [PubMed: 24837101]

16. Anderson DA 3rd, Dutertre CA, Ginhoux F & Murphy KM Genetic models of human and mouse dendritic cell development and function. Nat Rev Immunol 21, 101–115, doi:10.1038/s41577-020-00413-x (2021). [PubMed: 32908299]

17. Coombes JL et al. A functionally specialized population of mucosal CD103+ DCs induces Foxp3+ regulatory T cells via a TGF-beta and retinoic acid-dependent mechanism. The Journal of experimental medicine 204, 1757–1764, doi:10.1084/jem.20070590 (2007). [PubMed: 17620361]

18. Persson EK et al. IRF4 transcription-factor-dependent CD103(+)CD11b(+) dendritic cells drive mucosal T helper 17 cell differentiation. Immunity 38, 958–969, doi:10.1016/j.immuni.2013.03.009 (2013). [PubMed: 23664832]

19. Pool L, Rivollier A & Agace WW Deletion of IRF4 in Dendritic Cells Leads to Delayed Onset of T Cell-Dependent Colitis. J Immunol 204, 1047–1055, doi:10.4049/jimmunol.1900775 (2020). [PubMed: 31900340]

20. Wohn C et al. Absence of MHC class II on cDC1 dendritic cells triggers fatal autoimmunity to a cross-presented self-antigen. Science immunology 5, doi:10.1126/sciimmunol.aba1896 (2020).

21. Yamano T et al. Aire-expressing ILC3-like cells in the lymph node display potent APC features. The Journal of experimental medicine 216, 1027–1037, doi:10.1084/jem.20181430 (2019). [PubMed: 30918005]

22. Hepworth MR et al. Immune tolerance. Group 3 innate lymphoid cells mediate intestinal selection of commensal bacteria-specific CD4(+) T cells. Science 348, 1031–1035, doi:10.1126/science.aaa4812 (2015). [PubMed: 25908663]

23. Bartleson JM et al. Strength of tonic T cell receptor signaling instructs T follicular helper cell-fate decisions. Nature immunology 21, 1384–1396, doi:10.1038/s41590-020-0781-7 (2020). [PubMed: 32989327]

24. Mackley EC et al. CCR7-dependent trafficking of RORgamma(+) ILCs creates a unique microenvironment within mucosal draining lymph nodes. Nat Commun 6, 5862, doi:10.1038/ncomms6862 (2015). [PubMed: 25575242]

25. Kim MH, Taparowsky EJ & Kim CH Retinoic Acid Differentially Regulates the Migration of Innate Lymphoid Cell Subsets to the Gut. Immunity 43, 107–119, doi:10.1016/j.immuni.2015.06.009 (2015). [PubMed: 26141583]

26. Wang R et al. GARP regulates the bioavailability and activation of TGFbeta. Mol Biol Cell 23, 1129–1139, doi:10.1091/mbc.E11-12-1018 (2012). [PubMed: 22278742]

27. Lienart S et al. Structural basis of latent TGF-beta1 presentation and activation by GARP on human regulatory T cells. Science 362, 952–956, doi:10.1126/science.aau2909 (2018). [PubMed: 30361387]

28. Qin Y et al. A Milieu Molecule for TGF-beta Required for Microglia Function in the Nervous System. Cell 174, 156–171 e116, doi:10.1016/j.cell.2018.05.027 (2018). [PubMed: 29909984]

29. Lacy-Hulbert A et al. Ulcerative colitis and autoimmunity induced by loss of myeloid alphav integrins. Proc Natl Acad Sci U S A 104, 15823–15828, doi:10.1073/pnas.0707421104 (2007). [PubMed: 17895374]

30. Paidassi H et al. Preferential expression of integrin alphavbeta8 promotes generation of regulatory T cells by mouse CD103+ dendritic cells. Gastroenterology 141, 1813–1820, doi:10.1053/j.gastro.2011.06.076 (2011). [PubMed: 21745448]

31. Travis MA et al. Loss of integrin alpha(v)beta8 on dendritic cells causes autoimmunity and colitis in mice. Nature 449, 361–365, doi:10.1038/nature06110 (2007). [PubMed: 17694047]

32. Gardner JM et al. Deletional tolerance mediated by extrathymic Aire-expressing cells. Science 321, 843–847, doi:10.1126/science.1159407 (2008). [PubMed: 18687966]

33. Nakawesi J et al. alphavbeta8 integrin-expression by BATF3-dependent dendritic cells facilitates early IgA responses to Rotavirus. Mucosal Immunol 14, 53–67, doi:10.1038/s41385-020-0276-8 (2021). [PubMed: 32161355]

34. Brown CC et al. Transcriptional Basis of Mouse and Human Dendritic Cell Heterogeneity. Cell 179, 846–863 e824, doi:10.1016/j.cell.2019.09.035 (2019). [PubMed: 31668803]

35. Barnett LG et al. B cell antigen presentation in the initiation of follicular helper T cell and germinal center differentiation. J Immunol 192, 3607–3617, doi:10.4049/jimmunol.1301284 (2014). [PubMed: 24646739]

36. Hepworth MR et al. Innate lymphoid cells regulate CD4+ T-cell responses to intestinal commensal bacteria. Nature 498, 113–117, doi:10.1038/nature12240 (2013). [PubMed: 23698371]

37. Goto Y et al. Segmented filamentous bacteria antigens presented by intestinal dendritic cells drive mucosal Th17 cell differentiation. Immunity 40, 594–607, doi:10.1016/j.immuni.2014.03.005 (2014). [PubMed: 24684957]

38. Yin X, Chen S & Eisenbarth SC Dendritic Cell Regulation of T Helper Cells. Annu Rev Immunol 39, 759–790, doi:10.1146/annurev-immunol-101819-025146 (2021). [PubMed: 33710920]

39. Eberl G & Littman DR Thymic origin of intestinal alphabeta T cells revealed by fate mapping of RORgammat+ cells. Science 305, 248–251, doi:10.1126/science.1096472 (2004). [PubMed: 15247480]

40. Lochner M et al. In vivo equilibrium of proinflammatory IL-17+ and regulatory IL-10+ Foxp3+ RORgamma t+ T cells. The Journal of experimental medicine 205, 1381–1393, doi:10.1084/jem.20080034 (2008). [PubMed: 18504307]

41. Kaplan DH, Jenison MC, Saeland S, Shlomchik WD & Shlomchik MJ Epidermal langerhans cell-deficient mice develop enhanced contact hypersensitivity. Immunity 23, 611–620, doi:10.1016/j.immuni.2005.10.008 (2005). [PubMed: 16356859]

42. Dow LE et al. Conditional reverse tet-transactivator mouse strains for the efficient induction of TRE-regulated transgenes in mice. PLoS One 9, e95236, doi:10.1371/journal.pone.0095236 (2014).

43. Metzger TC et al. Lineage tracing and cell ablation identify a post-Aire-expressing thymic epithelial cell population. Cell Rep 5, 166–179, doi:10.1016/j.celrep.2013.08.038 (2013). [PubMed: 24095736]

44. Stoeckius M et al. Simultaneous epitope and transcriptome measurement in single cells. Nat Methods 14, 865–868, doi:10.1038/nmeth.4380 (2017). [PubMed: 28759029]

45. Stoeckius M et al. Cell Hashing with barcoded antibodies enables multiplexing and doublet detection for single cell genomics. Genome Biol 19, 224, doi:10.1186/s13059-018-1603-1 (2018). [PubMed: 30567574]

46. van Buggenum JA et al. A covalent and cleavable antibody-DNA conjugation strategy for sensitive protein detection via immuno-PCR. Sci Rep 6, 22675, doi:10.1038/srep22675 (2016). [PubMed: 26947912]

47. Hafemeister C & Satija R Normalization and variance stabilization of single-cell RNA-seq data using regularized negative binomial regression. Genome Biol 20, 296, doi:10.1186/s13059-019-1874-1 (2019). [PubMed: 31870423]

48. Hao Y et al. Integrated analysis of multimodal single-cell data. Cell 184, 3573–3587 e3529, doi:10.1016/j.cell.2021.04.048 (2021). [PubMed: 34062119]

49. Wolock SL, Lopez R & Klein AM Scrublet: Computational Identification of Cell Doublets in Single-Cell Transcriptomic Data. Cell Syst 8, 281–291 e289, doi:10.1016/j.cels.2018.11.005 (2019). [PubMed: 30954476]

50. Wolf FA, Angerer P & Theis FJ SCANPY: large-scale single-cell gene expression data analysis. Genome Biol 19, 15, doi:10.1186/s13059-017-1382-0 (2018). [PubMed: 29409532]

51. Lopez R, Regier J, Cole MB, Jordan MI & Yosef N Deep generative modeling for single-cell transcriptomics. Nat Methods 15, 1053–1058, doi:10.1038/s41592-018-0229-2 (2018). [PubMed: 30504886]
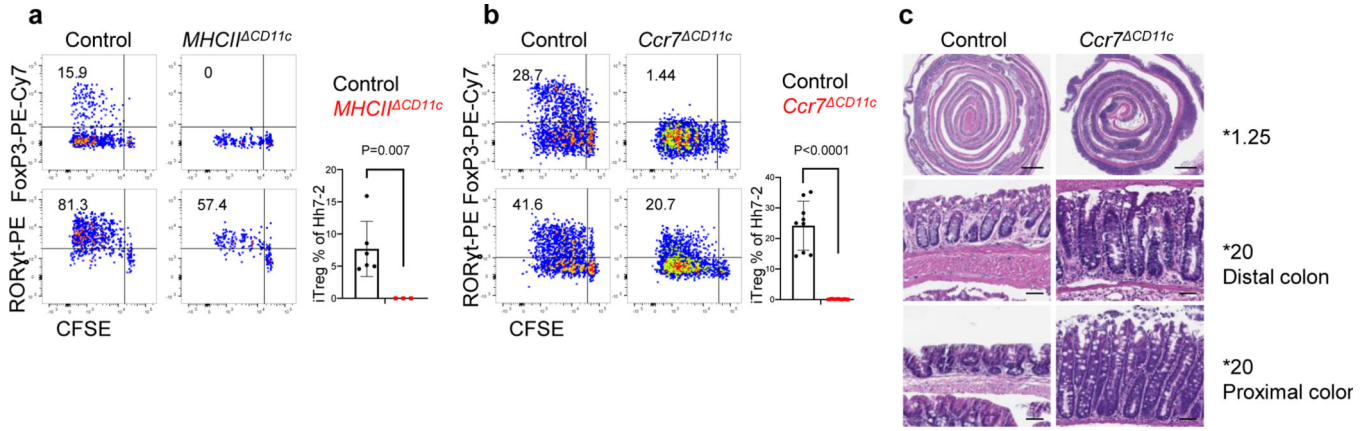
Figure 1. Distinct requirements for antigen presentation and CCR7 expression in differentiation of iTreg versus pathogenic Th17 cells.

a-b, Hh-specific T cell proliferation and differentiation in Hh-colonized $CD11c\text{-}Cre;I\text{-}Ab^{f/f}$ ($MHCII^{CD11c}$) (n=3) and $I\text{-}Ab^{f/f}$ or $CD11c\text{-}Cre;I\text{-}Ab^{f/+}$ littermate control mice (n=6) (a) and in $Ccr7^{CD11c}$ (n = 7) and littermate control mice (n = 9) (b). CFSE-labeled naïve TCR transgenic Hh7–2 T cells from the C1 MLN were assessed for cell proliferation and expression of FoxP3 and RORγt at 3 days after adoptive transfer. Representative flow cytometry (left) and aggregate results (right). Data summarize two (a) and three (b) independent experiments. **c,** Representative H&E histology in large intestine of mice with indicated genotypes. Scale bars are 1 mm and 50μm, for 1.25X and 20X. respectively. All statistics were calculated by unpaired two-sided Welch's t-test. Error bars denote mean ± s.d. p-values are indicated in the figure.
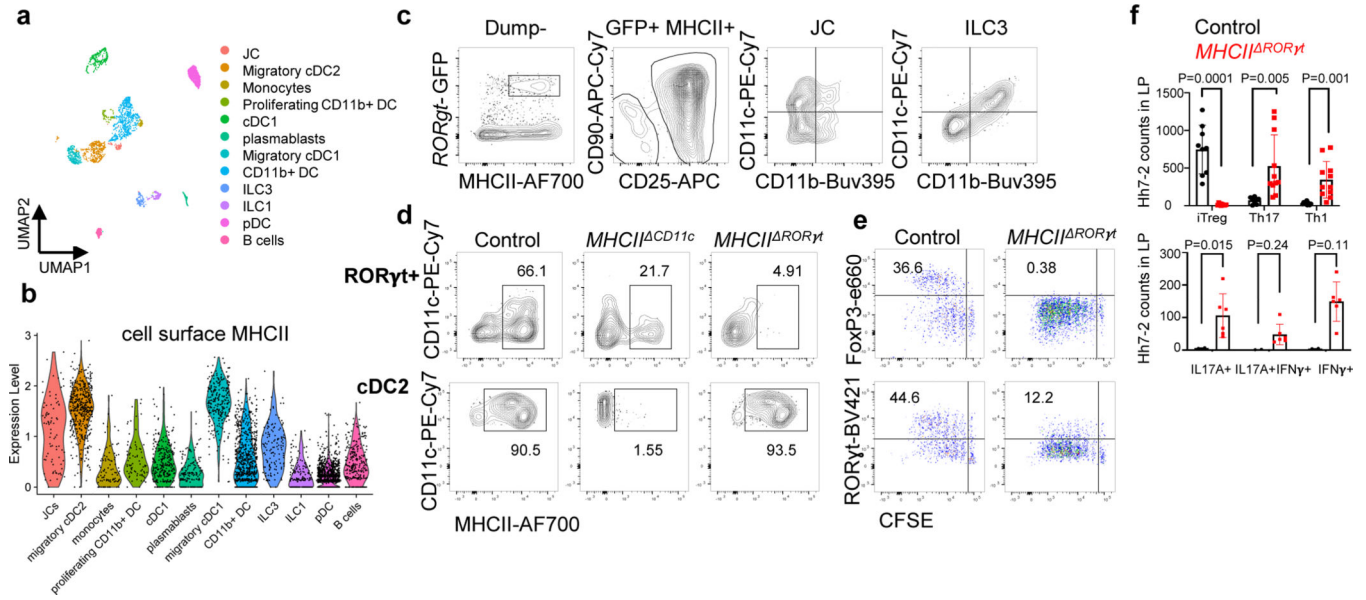
Figure 2. Antigen presentation by RORγt⁺ cells is required for microbiota-induced iTreg cell differentiation.

a-b, UMAP visualization of the *tdTomato-ON^{CD11c}* fate-map cell CITE-seq dataset, analyzed by the WNN method (a), and Violin plot showing MHCII protein levels in the different cell clusters (b). MLN cells from Hh-colonized *tdTomato-ON^{CD11c}* fate-map mice were gated for TCRβ⁻, TCRγδ⁻, B220⁻, and tdTomato⁺ cells were sorted for CITE-seq analysis. Cells were sorted from two mice and labeled by hashing antibodies (n=2). **c,** CD11c and CD11b staining of ILC3 and JC from MLN of Hh-colonized *RORγt-eGFP* mice, gated as indicated. **d,** MHCII expression in RORγt⁺ cells (top) and DCs (bottom) from the MLN of Hh-colonized mice of the indicated genotypes. RORγt⁺ cells were gated as TCRβ⁻, TCRγδ⁻, B220⁻, RORγt⁺; DC were gated as TCRβ⁻, TCRγδ⁻, B220⁻, CD90⁻, CD11c⁺, CD11b⁺ SIRPα⁺. **e,** Hh7–2 cell proliferation and differentiation in *MHCII^{RORγt}* (n = 6) and *I-Ab^{f/f}* littermate control mice (n = 6) at 3 days after adoptive transfer into Hh-colonized mice. **f,** Hh7–2 T cell differentiation profiles (upper) and cytokine production (lower) in the large intestine lamina propria at 22 days after transfer into *MHCII^{RORγt}* (n=11) and littermate controls (n=9). Differentiation was assessed by expression of Foxp3, RORγt with or without T-bet, and T-bet. Data summarize two independent experiments. All statistics were calculated by unpaired two-sided Welch's t-test. Error bars denote mean ± s.d. *p*-values are indicated on the figure.
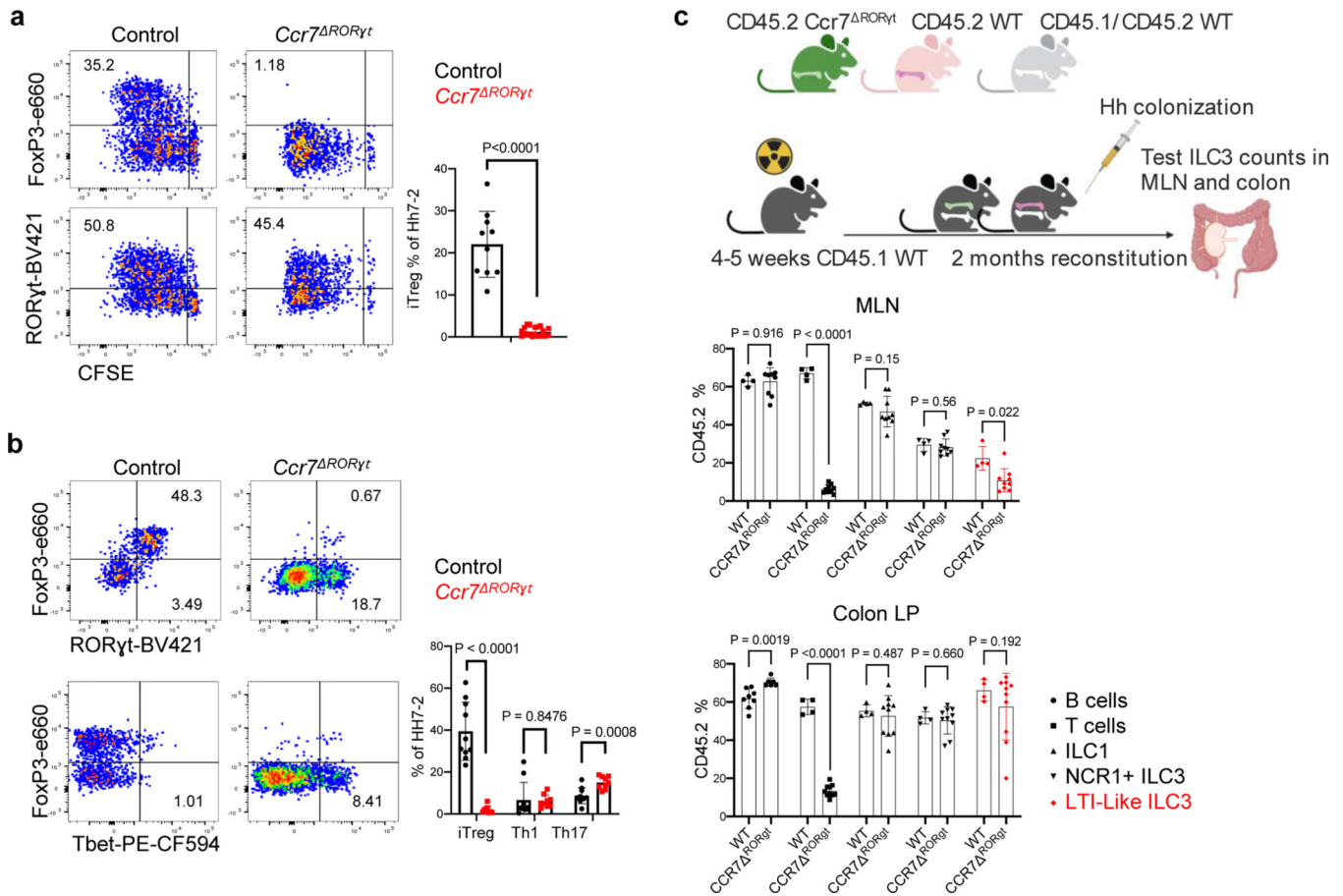
Figure 3. RORγt⁺ cells require CCR7 to promote iTreg cell differentiation.

a-b, Representative flow cytometry profiles (left) and aggregate data (right) for Hh7–2 T cell proliferation and differentiation in MLN at 3 days (a) and their phenotype in large intestine at 14 days (b) following adoptive transfer into *Ccr7* ^{RORγt} and littermate control mice. MLN: Control mice n=10, *Ccr7* ^{RORγt} mice n=20; LI: Control mice n=10, *Ccr7* ^{RORγt} mice n=9. Data summarize three independent experiments. Statistics were calculated by unpaired two-sided Welch's t-test. **c,** Analysis of CCR7 requirement for RORγt⁺ cell accumulation in the MLN. Irradiated CD45.1 mice were reconstituted with equal number of bone marrow cells from CD45.2 *Ccr7* ^{RORγt} and CD45.1/CD45.2 WT mice or with CD45.2 WT and CD45.1/CD45.2 WT mice as controls. Scheme is shown at the top (created with BioRender.com). Aggregate data shows the frequency in MLN and colon lamina propria of CD45.2 WT (n=4) or CD45.2 *Ccr7* ^{RORγt} (n=9) cells within each subset, as indicated. Data summarize three independent experiments. All statistics were calculated by unpaired two-sided Welch's t-test. Error bars denote mean ± s.d. *p*-values are indicated in the figure.
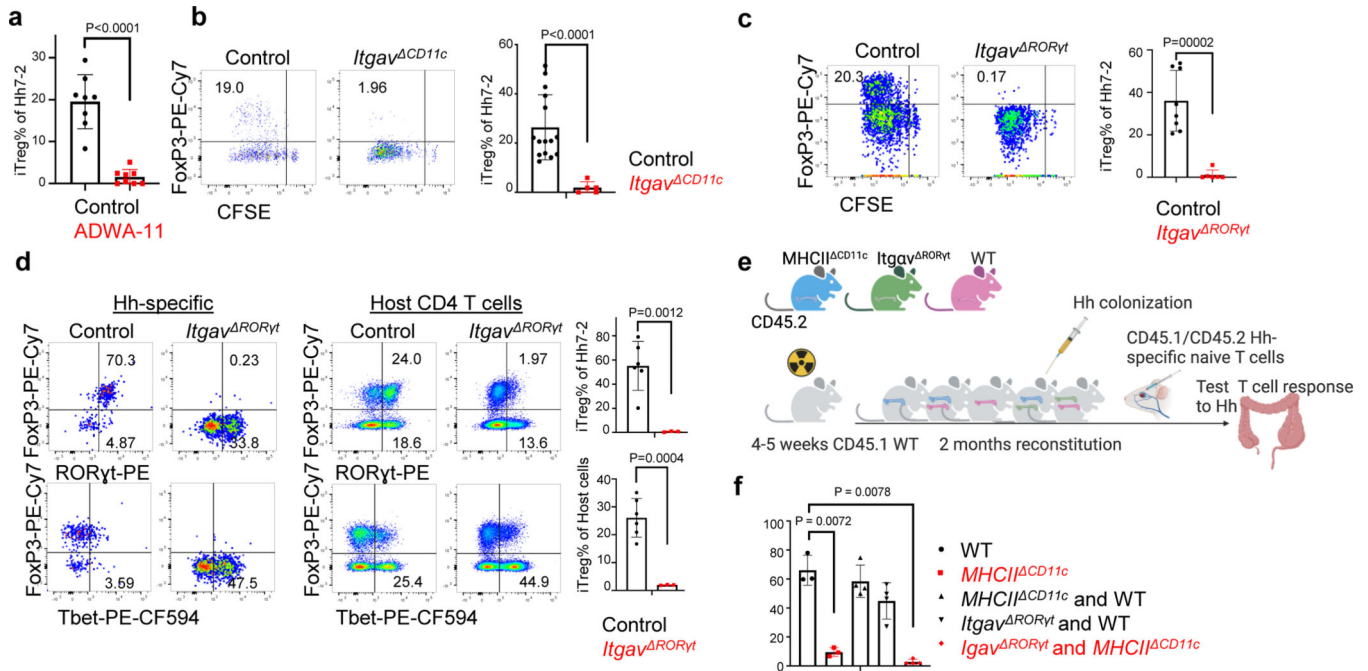
Figure 4. Role of integrin $\alpha_v\beta_8$ in RORγt$^+$ antigen presenting cell-dependent iTreg cell differentiation.

a, Frequency of iTreg cells among proliferating donor-derived Hh-specific cells in the MLN at 3 days after transfer of naïve CFSE-labeled Hh7–2 T cells into mice treated with 200μg of ADWA11 blocking antibody (n=8) or left untreated (n=8), on the day of adoptive transfer. Data summarize three independent experiments. **b,** Hh7–2 T cell proliferation and differentiation in the MLN of *Itgav* $^{\Delta CD11c}$ (n=5) and littermate controls (n=15) at 3 days after adoptive transfer. Data summarize three independent experiments. **c,** Proliferation and differentiation of Hh-specific iTreg cells in the MLN of *Itgav* $^{\Delta ROR\gamma t}$ (n=6) and littermate control mice (n=8). CFSE-labeled Hh7–2 T cells were analyzed at 3 days following their adoptive transfer into Hh-colonized mice. Representative flow cytometry profiles (left) and aggregate data (right). Data summarize three independent experiments. **d,** Transcription factor expression in Hh7–2 T cells (left panels) and in endogenous CD4$^+$ T cells (right panels) from colon lamina propria (LP) at 10 days after adoptive transfer into *Itgav* $^{ROR\gamma t}$ mice (n=3) and control littermates (n=6). Data summarize two independent experiments. Representative dot plots and aggregate data are shown (right panels). **e,** Scheme for mixed bone marrow chimeric mouse experiment, with control, *Itgav* $^{ROR\gamma t}$ or *MHCII* ^{CD11c} cells administered to irradiated host mice (created with BioRender.com). **f,** Bar graphs showing iTreg frequency among Hh7–2 T cells in the colon LP at 10 days after their transfer into the bone marrow chimeric mice, reconstituted with different combinations of donor cells as indicated. Control mice (n=3), *MHCII* ^{CD11c} (n=3), *MHCII* ^{CD11c} and WT (n=4), *Itgav* $^{ROR\gamma t}$ and WT (n=4) and *MHCII* ^{CD11c} and *Itgav* $^{ROR\gamma t}$ (n=4). All statistics were calculated by unpaired two-sided Welch's t-test. Error bars denote mean ± s.d. *p*-values are indicated in the figure.
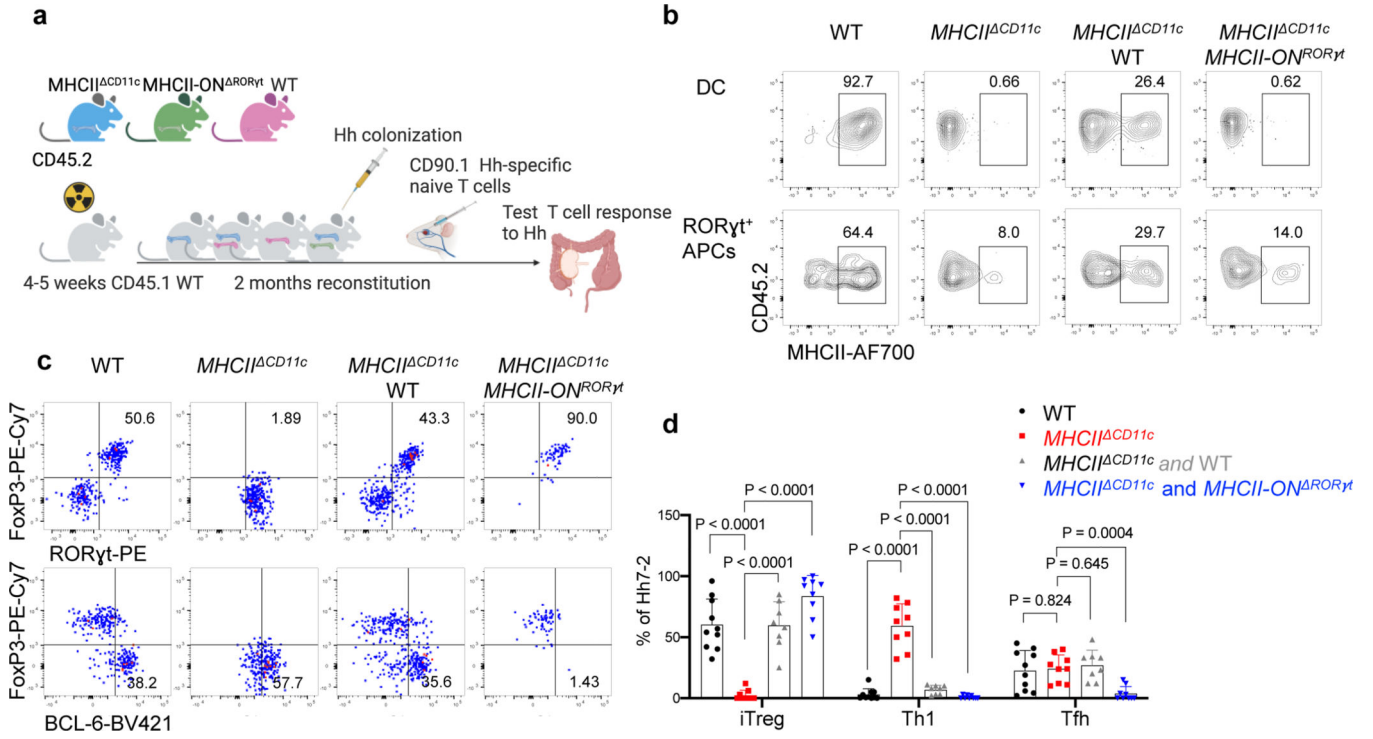
Figure 5. Antigen presentation by RORγt⁺ cells is sufficient to promote iTreg cell differentiation. a, Experimental design (created with BioRender.com). **b,** MHCII frequency in donor bone marrow-derived cDC2 (gated TCRβ⁻, TCRγδ, B220⁻, CD45.2⁺, CD11c⁺, CD11b⁺ Sirpa⁺) and RORγt⁺ cells (gated as TCRβ⁻, TCRγδ⁻, B220⁻, RORγt⁺, CD45.2⁺) in MLN from chimeric mice reconstituted with combinations of donor BM cells as indicated. **c,** Representative flow cytometry of Hh7–2 T cell differentiation in colon lamina propria of Hh-colonized bone marrow chimeric mice, 12 days after transfer of naive TCR transgenic T cells. **d,** Aggregate data for differentiation of Hh7–2 T cells in bone marrow chimeric mice reconstituted with cells of indicated genotypes. WT (n=10), MHCII *CD11c* (n=9), MHCII *CD11c* and WT (n=8), MHCII *CD11c* and MHCII-ON *RORγt* (n=9). Data summarize three independent experiments. All statistics were calculated by unpaired two-sided Welch's t-test. Error bars denote mean ± s.d. *p*-values are indicated in the figure.